EFFECT AND COMPENSATION OF COLORED TIMING JITTER IN PULSED UWB SYSTEM

POH BOON HOR

NATIONAL UNIVERSITY OF SINGAPORE

DEPARTMENT OF ELECTRICAL & COMPUTER ENGINEERING

2004/2005

EFFECT AND COMPENSATION OF COLORED TIMING JITTER IN PULSED UWB SYSTEM

POH BOON HOR
(B.Eng.(Hons.), NUS)

A THESIS SUBMITTED

FOR THE DEGREE OF MASTER OF ENGINEERING

DEPARTMENT OF ELECTRICAL & COMPUTER ENGINEERING

NATIONAL UNIVERSITY OF SINGAPORE

2004/2005

* This work was in part presented in the IEEE Joint UWBST & IWUWBS, Kyoto, Japan, May 2004.

ABSTRACT

Ultra Wideband systems impose a stringent requirement on the jitter performance of the system clock, which commonly exhibits colored timing jitter. This thesis firstly investigates the Bit Error Rate (BER) performance of a binary Pulse Position Modulation single-user UWB communication system subjected to colored timing jitter. Theoretical and simulation analyses show that colored jitter degrades BER performance more than white jitter, with greater degradation as jitter bandwidth decreases. Secondly a new jitter compensation algorithm is proposed to improve BER performance under colored timing jitter. It tracks the jitter by performing correlation between received signal and template and using the last decoded bit. This information is then used with known clock jitter bandwidth and jitter root-mean-square (RMS) value in deciding the current bit according to the maximum likelihood criterion. Simulation results show that it is effective in improving BER performance, with greater effectiveness as jitter bandwidth decreases and jitter RMS value increases.

Keywords: Ultra-wideband (UWB), colored timing jitter, maximum-likelihood (ML).

ACKNOWLEDGEMENTS

To the LORD God for His Grace and Mercy.

To Professor Ko Chi Chung, my supervisor, for his continuous support and guidance and encouragement in this project.

To Dr Francois Chin, my co-supervisor, for his support and understanding that make this project possible.

To Dr Zhi Wan Jun, for being patient and for the many advices and technical help in the first half of this project.

To Dr Huang Lei for his help in the review and drafting of the paper (arising from this work) submitted for IEEE Journal review.

To many Brothers and Sisters in Christ for all your prayers and support.

CONTENTS

ACKNOWLEDGEMENTS i
TABLE OF CONTENTS ii
SUMMARY iv
LIST OF TABLES vi
LIST OF FIGURES vii
LIST OF ABBREVIATIONS ix
LIST OF SYMBOLS x

CHAPTER 1 INTRODUCTION

1.1 Motivation 1
1.2 Objective & Contribution 2
1.3 Approach & Methodology 2
1.4 Summary of Results 3
1.5 Thesis Organization 4

CHAPTER 2 ULTRA WIDEBAND TECHNOLOGY

2.1 Introduction to UWB 6
2.2 Pulsed UWB Signal 6
2.3 Pulsed UWB Modulation 9
2.4 Time-Hopping UWB (TH UWB) 10
2.5 Advantages of Pulsed UWB 11
2.6 Disadvantages of Pulsed UWB 13
2.7 TH-UWB Transceiver Architecture 14

CHAPTER 3 VCO-PLL FREQUENCY SYNTHESIZERS

3.1 Chapter Overview 16
3.2 Crystal Oscillator, Voltage Controlled Oscillator & Phase Lock Loop 16
3.3 Phase Noise Characterization 17

CHAPTER 4 UWB SYSTEM MODEL & COLORED JITTER MODEL

4.1 Chapter Overview 20
4.2 Binary PPM Signaling with Timing Jitter 20
4.3 Binary PPM Bit Detection with Timing Jitter 23
4.4 Colored Jitter Phase Noise Model 25

CHAPTER 5 THEORETICAL ANALYSIS OF BER PERFORMANCE IN WHITE & COLORED TIMING JITTER

5.1 Chapter Overview 27

5.2 Effect of Timing Jitter in Bit Detection 27
5.3 BER Performance in White Timing Jitter 30
5.4 Effect of Colored Jitter Bandwidths on BER Performance 34
5.5 Upper and Lower Bounds for BER Performance in Colored Jitter 36

CHAPTER 6 FILTER DESIGN & GENERATION OF COLORED JITTER

6.1 Chapter Overview 38
6.2 Digital Filter Design (by Bilinear Transformation) 38
6.3 Time-Domain Representation of the Phase Noise Model 43
6.4 Generation of Colored Jitter 45
6.5 Verification of Generated Colored Jitter 48

CHAPTER 7 SIMULATION SETUP & RESULTS

7.1 Chapter Overview 50
7.2 Simulation Setup and Parameters 50
7.3 Statistical Validity 52
7.4 BER Performance in White Gaussian Jitter 52
7.5 BER Performance in Colored Gaussian Jitter 54

CHAPTER 8 JITTER COMPENSATION ALGORITHM

8.1 Chapter Overview 55
8.2 Motivation and Approach 55
8.3 Jitter Tracker 58
8.4 Jitter Estimator 61
8.5 Optimal ML Decision Rule 64
8.6 Performance Evaluation & Discussion 69
8.7 Computation Complexity of the proposed Jitter Compensation Algorithm 71

CHAPTER 9 CONCLUSION AND FUTURE WORKS

9.1 Conclusion 72
9.2 Future Works 73

BIBLIOGRAPHY 74

SUMMARY

Ultra Wideband (UWB) is a promising technology in wireless communications and geolocation. The narrowness of the UWB pulses gives UWB many advantages over existing technology but also imposes a high requirement on the jitter performance of the system clock. Much research has been done on the performance of UWB systems however few results are available in literature on the effects of timing jitter on UWB performance. In practical systems, the system clock is a frequency synthesizer implemented in a closed-loop Voltage Controlled Oscillator-Phased Locked Loop (VCO-PLL) hybrid. Such a clock exhibits colored (correlated) timing jitter instead of white jitter and the extent of correlation affects the Bit Error Rate (BER) performance.

The contribution of this thesis is two fold. Firstly the BER performance of a binary Pulse Position Modulation (PPM) single-user pulsed UWB communication system subjected to both white and colored clock timing jitters is investigated. In such schemes, multiple pulses are used to represent a single information bit. The system clock is modeled by a phase noise model having two basic parameters: jitter root-mean-square (RMS) value and jitter bandwidth. Theoretical analysis shows that BER performance in colored jitter (for a fixed number of pulses per bit) is lower bounded by that of the white jitter case (for the same number of pulses per bit) and upper bounded by that of the case where a single pulse is used to represent one bit, agreeing with the simulation results. Moreover it is found that clocks with lower jitter bandwidth degrade the BER performance more than those with higher jitter bandwidth.

The second contribution of this thesis is the proposal of a new jitter compensation algorithm which improves the BER performance of pulsed UWB systems subjected to colored Gaussian timing jitter. The proposed algorithm attempts to track first the jitter by making use of the correlation between the transmitted pulse-train representing the present bit and the receiver template as well as the last decoded bit. This information is then used together with the assumed known clock jitter characteristics (jitter bandwidth and jitter RMS value) in the decision making of the current bit according to the maximum likelihood criterion. Simulation results show that the algorithm is effective in improving the BER performance and the performance is better as the jitter bandwidth decreases and as the jitter RMS value increases.

LIST OF TABLES

Table 5.1 *Tabulation of Probability of Error in White Gaussian Jitter, for N_f =100 pulses per bit* 33

LIST OF FIGURES

Figure 2.1	*Gaussian Monocycle Waveform and PSD*	7
Figure 2.2	*Scholtz's Monocycle Waveform and PSD*	8
Figure 2.3	*Time-shifted Monocycles according to $c_i T_h$ and $b\,\delta$*	11
Figure 3.1	*Block Diagram of a Basic VCO-PLL Frequency Synthesizer*	17
Figure 3.2	*Typical Circuit to Measure Phase Noise*	18
Figure 4.1	*Bit information encoded onto Scholtz's monocycle positions*	21
Figure 4.2:	$R_p(\tau)$, pulse correlation function of *p*(t)	22
Figure 4.3	Effect of timing jitters on the monocycle positions	23
Figure 4.4	*Binary PPM correlation template v(t) for N_f = 1 pulse per bit.*	24
Figure 4.5	*Binary PPM correlation template, v(t) for N_f = 4 pulses per bit*	24
Figure 4.6	*Colored Jitter Phase Noise Model*	26
Figure 5.1	*Pulse-template correlation function*	28
Figure 5.2	*Two Gaussian PDFs of the same mean but different variance*	35
Figure 5.3	*Upper and lower bound for BER performance in colored timing jitter for N_f = 100 pulses per bit*	37
Figure 6.1	*Phase Noise Model*	39
Figure 6.2	*Bode Magnitude Plot of Analogue Filter H(s)*	40
Figure 6.3	*Bode Magnitude Plot of Digital Filter H(z)*	42
Figure 6.4	*A realization of generated colored timing jitter, f_l = 1e5 Hz* and $\varepsilon_{rms} = 25\,ps$.	47

Figure 6.5	*A realization of generated colored timing jitter, f_l = 1e6 Hz* and $\varepsilon_{rms} = 25\,ps$	48
Figure 6.6	*Estimated PSD of Generated Colored Jitter*	49
Figure 7.1	*Scholtz Monocycle with T_n = 0.29ns*	51
Figure 7.2	*BER Performance in White Gaussian Jitter for 100 pulses per bit*	53
Figure 7.3	*BER Performance in White Gaussian Jitter for 1 pulse per bit*	53
Figure 7.4	*BER Performance in Colored Gaussian Jitter for N_f = 100 pulses per bit*	54
Figure 8.1	*Original receiver without jitter compensation*	56
Figure 8.2	*New receiver with jitter tracking and compensation*	57
Figure 8.3	*Approximation for jitter waveform (a) $f_L = 10^4$ Hz, (b) $f_L = 10^7$ Hz*	59
Figure 8.4	*Resolving ambiguity for ε_n using three templates*	61
Figure 8.5	*Probability Distribution Function of e_{n+1}*	64
Figure 8.6	*Probability density functions of d_{n+1} when e_n =0, 56 and 95 ps and the associated decision thresholds and regions.*	67
Figure 8.7	*BER performance after jitter compensation*	70

LIST OF ABBREVIATIONS

BER	Bit Error Rate
FCC	Federal Communications Commission
ML	Maximum-Likelihood
OOK	On-Off Keying
PAM	Pulse Amplitude Modulation
PD	Phase Detector
PDF	Probability Density Function
PLL	Phase Locked Loop
PPM	Pulse Positioning Modulation
PSD	Power Spectral Density
RMS	Root-Mean-Square
TH-UWB	Time Hopping Ultra Wideband
UWB	Ultra Wideband
VCO	Voltage Controlled Oscillator

LISTS OF SYMBOLS

?	Delay of the template in the receiver to resolve jitter ambiguity
σ_x^2	Power of the white Gaussian noise used to generate the colored jitter
a	Bilinear filter coefficient
b_n	n^{th} information bit
$\hat{b}_n$	Estimate for the n^{th} information bit
δ	Binary PPM modulation parameter to encode bit information
d_n	Decision variable for the n^{th} bit
$d_{\Delta n}$	Decision variable for the n^{th} bit when using the delayed template
ε	Timing jitter, in units of second
ε_ϕ	Phase jitter, in units of radian
ε_{rms}	Root-mean-square timing jitter, in units of second
$\varepsilon_{\phi,rms}$	Root-mean-square phase jitter, in units of radian
ε_i	Timing jitter associated with the i^{th} pulse
ε_n	Timing jitter associated with the n^{th} bit
$\hat{\varepsilon}_{n+1}$	Estimated timing jitter associated with the $n+1^{th}$ bit
f_c	Oscillator nominal frequency
f_L	3dB bandwidth of phase noise, also jitter bandwidth
f_s	Sampling frequency of the filter

N_f	Number of pulses per bit
N_{floor}	Inband noise floor of the phase noise
$p(t)$	UWB pulse
P_e	Probabiliy of bit error
$r(t,n)$	Received signal
$R_p(t)$	Pulse correlation function
$R(t)$	Pulse-template correlation function
$s(t,n)$	Transmitted signal
$S_\phi(f)$	Phase noise power spectral density
T_f	Frame time
T_n	Constant that determines Monocycle's Duration
$v(t)$	Correlation Template

CHAPTER 1

INTRODUCTION

1.1 Motivation

Ultra Wideband (UWB) is a promising technology in wireless communications and geolocation. Using low duty cycle subnanosecond pulses, pulsed UWB systems promise good multipath resistance [1][2]. The narrowness of the UWB pulses, the very characteristic that gives UWB its many advantages also imposes a high requirement on the jitter performance of the system clock. The recent UWB research focuses on signal design [3], multiple access performance [1][2], channel modeling and estimation [4][5], modulation and coding scheme [6][7], receiver structure [8], and interference issues [9][10]. However, apart from [11] where the effect of white Gaussian timing jitter was investigated through simulations only, few results are available in the literature on the effect of timing jitter on UWB performance.

In practical systems, the system clock is a frequency synthesizer implemented as a hybrid of the voltage-controlled oscillator (VCO) and phased-locked loop (PLL). Such a clock exhibits colored timing jitter instead of white jitter. In other words, its phase noise is not flat over all frequencies and successive jitter samples are correlated. The extent of correlation is related to the PLL bandwidth, and would degrade the bit error rate (BER) performance. Motivated by this, the BER performance of a pulsed UWB system in the presence of colored timing jitter is investigated in this thesis and a jitter compensation algorithm is proposed to improve BER performance.

1.2 Objective & Contribution

The objective and contribution of this thesis is two-fold: Its first contribution is to investigate the BER performance of a single-user binary pulse position modulation (PPM) UWB system subjected to both white and colored clock timing jitters. The second contribution is to propose a new jitter compensation algorithm which improves the BER performance of pulsed UWB systems subjected to colored Gaussian timing jitter.

1.3 Approach & Methodology

The BER performance is investigated via both theoretical analysis as well as simulation. A jitter phase noise model having two basic parameters: jitter root-mean-square (RMS) value and jitter bandwidth [12] is adopted. The colored jitter is modeled as the output from filtering white Gaussian noise with a digital filter designed from the phase noise model by bilinear transformation. The BER performance is analyzed theoretically by considering how the error probability is affected by the jitter. For the simulations, the jitter RMS value is varied (from 0 to 180ps) and the resulting BER obtained for colored jitter of different bandwidths (10KHz to 10MHz and including white jitter) is plotted to produce a family of BER curves (BER against jitter RMS value) for different jitter bandwidths.

Timing jitter has noise-like behavior and has often been treated as non-amenable to compensation. For colored or correlated timing jitters, it is conceivable that some sort of compensation is possible if the decision rule takes into account the jitter characteristics (jitter RMS value and jitter bandwidth) of the system clock. The proposed algorithm attempts to track first the jitter by making use of the correlation between the transmitted

pulse-train representing the present bit and the receiver template as well as the last decoded bit. This information is then used together with the assumed known clock jitter characteristics (jitter bandwidth and jitter RMS value) in the decision making of the current bit according to the maximum likelihood (ML) criterion.

1.4 Summary of Results

Theoretical analysis shows that BER performance in colored jitter (for a fixed number of pulses per bit) is lower bounded by that of the white jitter case (for the same number of pulses per bit) and upper bounded by that of the case where a single pulse is used to represent one bit, agreeing with the simulation results. It is also shown that clocks with lower jitter bandwidth degrade the BER performance more than those with higher jitter bandwidth. From the simulations, a jitter RMS value of 105ps for white jitter results in a BER of 10^{-3}, while for colored jitter with a 3 dB bandwidth of 100kHz, a significantly smaller jitter RMS value of about 25ps results in the same BER

A jitter compensation algorithm is proposed to improve the BER performance degradation due to colored jitter. Simulation results show that the algorithm is effective in improving the BER performance and the performance is better as the jitter bandwidth decreases and as the jitter RMS value increases. This is as expected as the algorithm tracks the jitter and exploits the correlation in the jitter which is more significant at lower bandwidths. A BER improvement of approximately one order of magnitude is achieved for jitter with bandwidth of 10^4 Hz and jitter RMS value beyond 40 ps.

1.5 Thesis Organization

Chapter 2 presents background information on UWB technology. It summaries Pulsed UWB signal characteristics and modulation techniques. The advantages and disadvantages associated with UWB in comparison to conventional systems are also discussed.

Chapter 3 provides basic information about VCO-PLL frequency synthesizers and phase noise (frequency domain of timing jitter) characterization.

Chapter 4 describes the single-user PPM UWB system model with clock timing jitter incorporated in the model and the colored jitter phase noise model used in this thesis.

Chapter 5 presents the theoretical analysis of the BER performance in white and colored timing jitter.

Chapter 6 describes the design of a digital filter by bilinear transformation based on the phase noise model and the generation of colored Gaussian timing jitter used in the simulations.

Chapter 7 describes the simulation setup and presents simulation results of the BER performance in white and colored timing jitter.

Chapter 8 derives the proposed jitter compensation algorithm which is used to improve BER performance and evaluates via simulations the effectiveness of the proposed jitter compensation algorithm in improving BER performance.

Chapter 9 concludes the thesis and recommends possibilities for future works.

CHAPTER 2

ULTRA WIDEBAND TECHNOLOGY

2.1 Introduction to UWB

Ultra wideband technology (UWB) commonly includes pulsed UWB or Orthogonal Frequency Division Multiplexing. This thesis is only concerned with Pulsed UWB. Pulsed UWB essentially involves the generation, transmission and reception of short-duration electromagnetic pulses, instead of sinusoids. It was first used in radar systems and has recently generated much research interest in the communications field [1-10]. Its very wide bandwidth and baseband nature (no carrier) results in many benefits such as multipath resistance, better material penetrating properties, higher data rates and lower system complexity. Despite these, the narrowness of the UWB pulses, the very characteristic that gives UWB its many advantages also imposes a high requirement on the jitter performance of the system clocks.

This chapter provides an overview of UWB signal characteristics, various modulation techniques as well as the advantages and disadvantages associated with UWB in comparison to conventional systems.

2.2 Pulsed UWB Signal

The Federal Communications Commission's definition for UWB is any signal with 25% or more fractional bandwidth. Fractional Bandwidth is the ratio of a signal's 10dB bandwidth to its center frequency. In April 2002, a new order state that it must

meet the spectrum mask of 2.4000-2.4835 GHz, 5.15-5.35GHz and 5.75-5.85GHz [13]. Any signal that fulfils these requirements may be considered UWB. UWB signals can be modeled by impulse-shaped mathematical functions known as monocycles. The 2 types of monocycles popular in literature are the Gaussian monocycle [14] and the Scholtz's monocycle [2].

2.2.1 Gaussian monocycle

The Gaussian monocycle can be represented by

$$p(t) = \frac{t}{T_n} e^{-2\left[\frac{t}{T_n}\right]^2} . \tag{2.1}$$

Its waveform and power spectral density, with T_n = 0.29 ns is illustrated in Figure 2.1. The resulting pulse has a very narrow duration of less than 1 ns and a very wide 3 dB bandwidth from about 1 to 3 GHz.

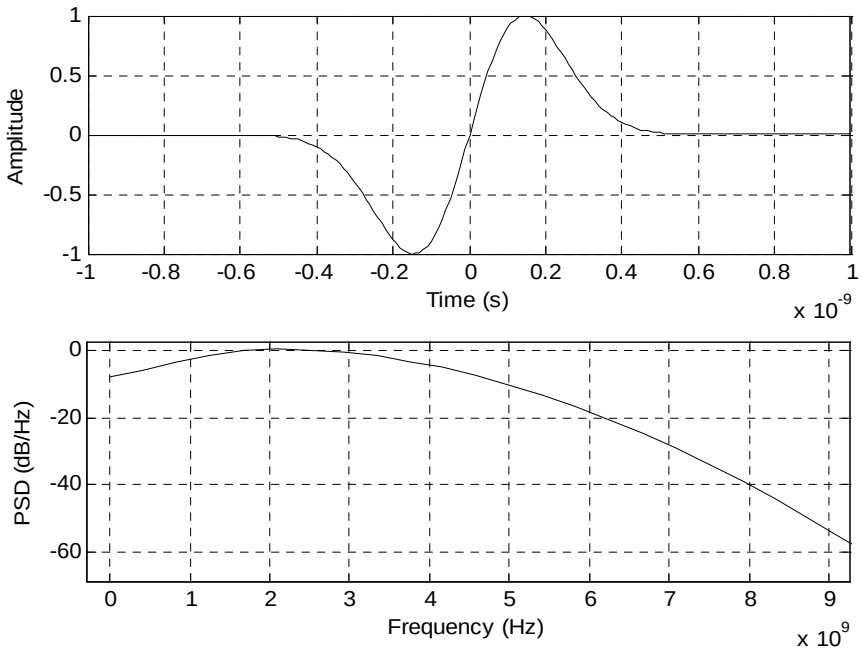

Figure 2.1: Gaussian Monocycle Waveform and PSD

2.2.2 Scholtz's Monocycle

The Scholtz's monocycle is similar to the second derivative of the Gaussian Pulse, and can be represented by

$$p(t) = \left[1 - 4\pi\left(\frac{t}{T_n}\right)^2\right] e^{-2\pi\left[\frac{t}{T_n}\right]^2}. \tag{2.2}$$

Its waveform and power spectral density, with T_n = 0.29ns is illustrated in Figure 2.2. The resulting pulse has a very narrow duration of less than 1 ns and a very wide 3 dB bandwidth from about 2 to 4 GHz.

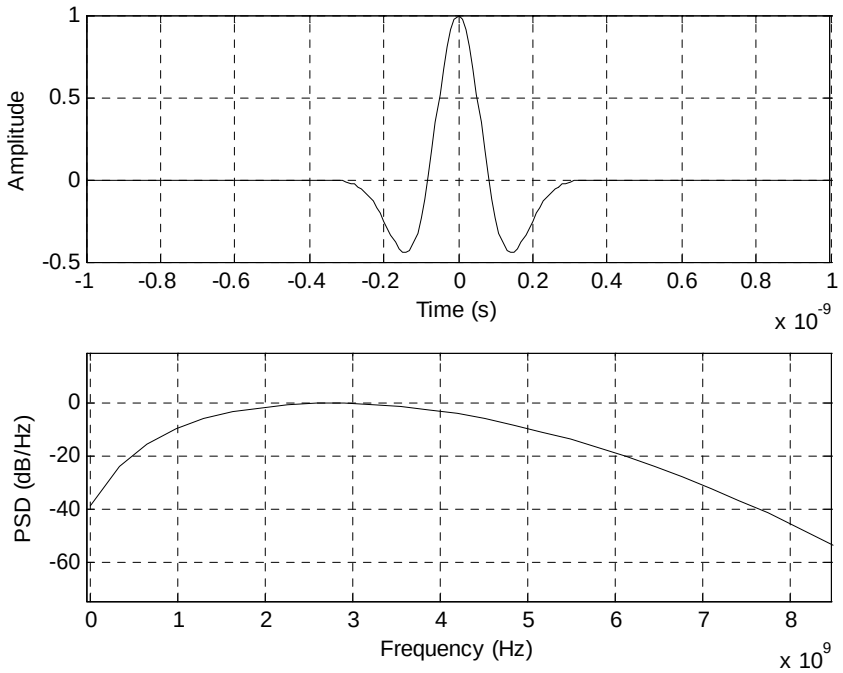

Figure 2.2: Gaussian Monocycle Waveform and PSD

2.3 Pulsed UWB Modulation

Various types of modulation techniques are possible including monophase techniques such as Pulse Position Modulation (PPM), Pulse Amplitude Modulation (PAM), On-Off Pulse Keying (OOK) as well as Bi-Phase Modulation. PPM encodes bit information by modifying the position of the transmitted monocycle. PAM modifies the magnitude of the monocycle based on the bit information. OOK codes a ‘0’ by the absence of a pulse. Bi-Phase Modulation reads forward and backward pulses as either ‘1’s or ‘0’s. Hybrid modulation techniques are also possible such as those incorporating both PAM and PPM.

2.4 Time-Hopping UWB (TH UWB)

A popular signaling format is the Time-Hopping UWB (TH UWB) scheme as described in [2]. It modulates using PPM and incorporates spread spectrum concepts by using pseudorandom TH sequences to reduce multiple access interference.

A typical TH format is given by

$$s^{(k)}(t) = \sum_{i=0}^{N_f-1} p(t - iT_f - c_i^{(k)}T_h - b^{(k)}\delta) \tag{2.3}$$

where $s^{(k)}(t)$ is the transmitted signal of the k^{th} transmitter made up of a summation of time-hopped monocycle pulses to form a pulse train. N_f is the number of monocycles used in representing a single bit. T_f is the frame time or nominal pulse repetition time. To minimize multiple access interference, each user is assigned a unique code sequence $c^{(k)}$, and $c_i^{(k)}T_h$ determines the additional time-shift added to the i^{th} monocycle. Each information bit is encoded in the pulse train by delaying the N_f monocycles by an additional amount $b^{(k)}\delta$. The duty cycle of the pulse train is the ratio of the monocycle width to T_f. It is typically 0.01 or less. Figure 2.3 illustrates how each monocycle is time shifted according to $c_i^{(k)}T_h$ and $b^{(k)}\delta$.

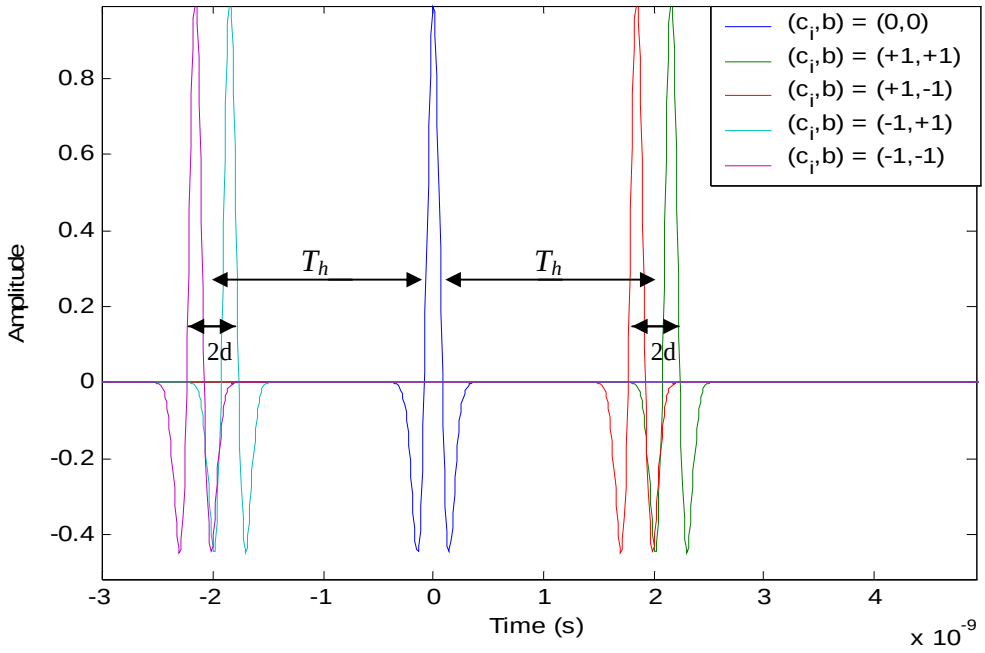

Figure 2.3: Time-shifted Monocycles according to $c_i T_h$ and $b\,\delta$

2.5 Advantages of Pulsed UWB

UWB can resolve the multipath propagation problem because of its very fine time resolution capability made possible by its very narrow (subnanosecond) monocycles. The time resolution is dependent on the pulse width and for a typical UWB pulse width of less than 1 ns, it corresponds to a path differential of 30 cm. Hence UWB can exploit the diversity inherent in a dense multipath channel. Furthermore, it has been reported in [16] that UWB signals do not suffer from multipath in the indoor environment of a typical office building. The narrow pulse width also makes UWB a good candidate for radar and geolocation applications. Achieving high resolution is of primary importance in these applications. Here distance can be determined by measuring the time delay of a pulse from transmitter to receiver. The resolution of the measurement is inversely proportional

to the pulse width. A range resolution in the order of centimeters has been demonstrated in UWB systems [17].

Because of the low duty cycle of UWB pulse train (the ratio of the pulse width to the frame time is typically less than 0.01), it has an inherent advantage in the multi-user channel. With the use of time-hopping codes, each user suffers less interference from other users. The low duty cycle also implies low power consumption for UWB devices. This is of practical importance in UWB applications such as geolocation tags to localize items in an enclosed environment such as in a warehouse. In such applications efficient power usage is needed because the light weight nature of the geolocation tags preclude large battery. Another reason is to minimize recharging hassle.

Furthermore as a result of its wide bandwidth, the spectral energy density of UWB signals in any narrow band is quite small and indistinguishable from noise. These result in low probability of intercept, something that is of great interest to military applications where detection avoidance is important. Electronic warfare aside, another chief benefit is minimal interference with other applications such as that of the GSM system and the GPS system. The low spectral energy density also results in minimal RF health hazards [18].

Lastly, the wide bandwidth of UWB signals are directly generated unlike that of spread spectrum signals, which are really narrow band signal made wideband by pseudo-random coded spreading waveform. Due to its carrier-free baseband nature, unlike carrier-based spread spectrum systems which have a complex implementation (with PseudoRandom Code Generator, RF/IF conversion stages, local oscillators, mixers,

filters, high chip rate modulators), UWB systems require minimal RF circuitry resulting in lower system complexity and cost. Furthermore because of their baseband nature, they have better material penetrating capabilities (e.g. through walls) than signals modulated to carriers with higher frequencies [18]. This may be exploited in applications where there is a need to “see” through barriers, for example, in the rapid scanning and detection of sensitive items in cargoes containers.

2.6 Disadvantages of Pulsed UWB

The chief drawback of UWB is also the same feature that gives it many advantages: its ultra-wide bandwidth. UWB devices have to be power limited (compared to narrowband technology which is bandwidth limited) because they must coexist on a non-interfering basis with other licensed and unlicensed users across several frequency bands. Global Positioning System providers have serious reservations about UWB systems that introduce even very low levels of interference into the 1.2GHz and 1.5GHz bands of its dual carrier.

Nonetheless the FCC gave the go ahead stating that UWB devices for measurement and communications must operate with their –10 dB bandwidth in the frequency band 3.1-10.6 GHz. Emission levels from UWB device must also meet an emissions mask at ISM 2.4GHz and U-NII at 5GHz within and below the 3.1-10.6GHz.[13] This may be done with spectrally filtered UWB, such as that patented by Multispectral Solutions, Inc. Also it was recently realized that multi-bands technique [15] can be modified for use with the UWB spectrum. The idea is to use multiple frequency bands which avoid the emission masks to efficiently utilize the UWB spectrum by

transmitting multiple UWB signals at the same time. The Orthogonal Frequency Multiplex Division method is an example of this technique that is currently a popular research topic.

Other problems include that of sampling at the receiver end. Ultra high-speed (in excess of 1 GHz) and precise samplers are required to properly sample a waveform having duration in the order of nanoseconds. The effect of timing jitter also leads to significant degradation in performance due to the fact that UWB uses very narrow pulses to convey information. This problem was investigated in [11] and is also the subject of this thesis. Furthermore, high speed data recorders and huge data storage memory are needed in actual implementations. These represent a great demand in the hardware in terms of cost and complexity.

2.7 TH-UWB Transceiver Architecture

Time Domain Corp has patented PulsON® silicon solutions based on UWB technology which enables new capabilities in communications, precision positioning and radar sensing [19]. PulsON® transmitters emit ultra-short monocycles (0.2 to 1.5 nanoseconds) with tightly controlled pulse intervals (25-1000 nanoseconds). Their transmitter uses Pulse Positioning Modulation (PPM), which varies the precise timings of the transmission of a monocycle about the nominal position to modulate data unto the monocyles.

For this transceiver block diagram, the timing uncertainty is at the Pulse Generators of both the transmitter and receiver, which determines the time position of

each monocycle in the transmitted monocycle pulse train. This thesis and also earlier work in [11] investigate the effects of timing jitter in such a transceiver structure.

CHAPTER 3

VCO-PLL FREQUENCY SYNTHESIZERS

3.1 Chapter Overview

This chapter provides basic information about clocks derived from Voltage Controlled Oscillators (VCO) in Phase Lock Loop (PLL). The characterization of their phase noise (spectral density of timing jitter) is described.

3.2 Crystal Oscillator, Voltage Controlled Oscillator and Phase Locked Loop

Quartz crystal oscillators have excellent frequency stability but they are not practical for applications that need a range of operating frequencies, since a specific crystal produces only harmonics of its fundamental frequency. On the other hand, voltage controlled oscillators produce a periodic signal whose frequency changes over a larger range in response to an external voltage, but its spectral purity is not as pure as that of crystal oscillators. This is because any slight voltage variation in the VCO circuit causes the frequency to shift.

Both the frequency stability of the crystal oscillator and the frequency flexibility of the VCO can be combined to form a better frequency synthesizer using the phase lock loop. Essentially the PLL is a closed loop feedback system that compares the outputs of the VCO and the crystal oscillator using a phase detector (PD). The output of the PD is a

DC voltage, which varies in magnitude according to the phase differences between its two input signals. The PD output is fed back to the VCO as a correction voltage to drive the output of the VCO towards the more stable crystal oscillator frequency.

By using frequency dividers in the PLL circuit to divide the frequency of the VCO output, $F_{Out,}$ stable multiples of the crystal oscillator frequency, F_{Ref}, can be achieved at the VCO output. High frequency clocks normally use a PLL to 'up' the frequency of a reference quartz crystal, F_{Ref}. The F_{Out} at the VCO output is used to provide the timing signal for other circuitry. The Figure 3.1 shows the basic block diagram of a VCO-PLL frequency synthesizer.

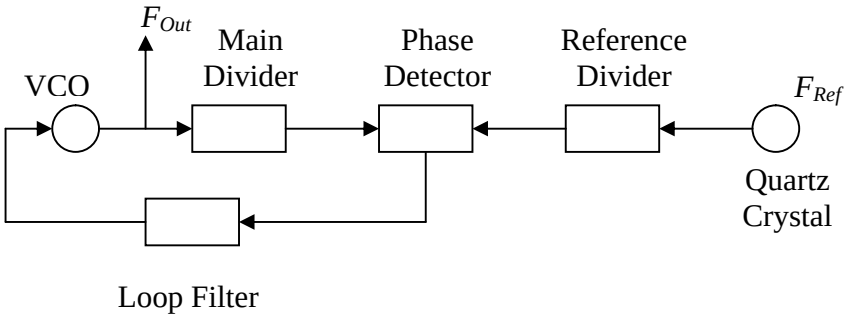

Figure 3.1: Block Diagram of a Basic VCO-PLL Frequency Synthesizer

3.3 Phase Noise Characterization

An ideal noiseless oscillator can be represented as

$$V(t) = A\sin(2\pi f_c t) \tag{3.1}$$

where A is the amplitude and f_c is the synthesizer nominal oscillating frequency. A noisy oscillator can be modeled by

$$V(t) = A\left(1+\alpha(t)\right)\cdot\sin\left(2\pi f_c t + \varepsilon_\phi(t)\right) \tag{3.2}$$

where $\alpha(t)$ is introduced as the amplitude modulation noise, $\varepsilon_\phi(t)$ is the phase modulation noise and f_c is the synthesizer nominal frequency. The time jitter $\varepsilon(t)$, in units of seconds, is related to phase jitter $\varepsilon_\phi(t)$, in units of radians by

$$\varepsilon(t) = \frac{\varepsilon_\phi(t)}{2\pi}\cdot\frac{1}{f_c} \quad . \tag{3.3}$$

The phase noise of a frequency synthesizer is the spectral density $S_\phi(f)$ of the time domain phase jitter $\varepsilon_\phi(t)$, and may be easily measured with a spectrum analyzer. Figure 3.2 shows a typical circuit to measure phase noise.

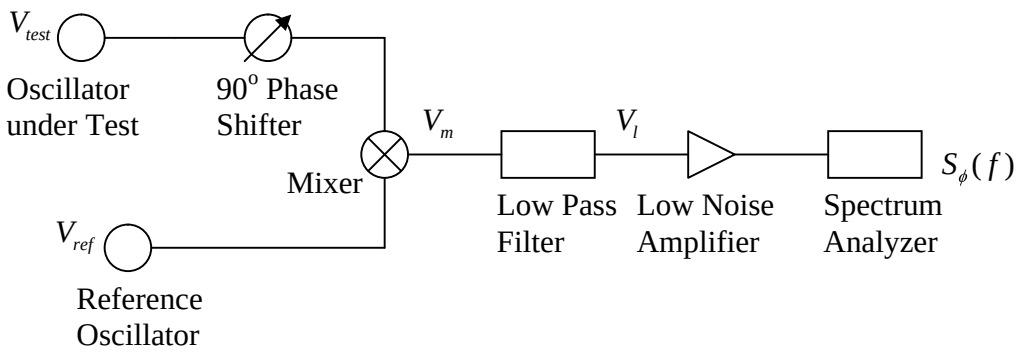

Figure 3.2: Typical Circuit to Measure Phase Noise

The Reference Oscillator and the Test Oscillator have the same nominal frequency, f_c. Assuming that the amplitude noise modulation is small and negligible, they are respectively represented by

$$V_{ref}(t) = A\sin(2\pi f_c t) \tag{3.4}$$

$$V_{test}(t) = A\sin(2\pi f_c t + \varepsilon_\phi(t)). \tag{3.5}$$

After the phase shifter, at the input to the mixer:

$$V_{ref}(t) = A\sin(2\pi f_c t) \tag{3.6}$$

$$V_{test}(t) = A\cos(2\pi f_c t + \varepsilon_\phi(t)) \tag{3.7}$$

At the output of mixer:

$$V_m(t) = \frac{A^2}{2}\left(\sin[4\pi f_c t + \varepsilon_\phi(t)] + \sin[\varepsilon_\phi(t)]\right) \tag{3.8}$$

After the LPF:

$$V_l(t) = K \cdot \sin[\varepsilon_\phi(t)] \tag{3.9}$$

where K is a constant. For small $\varepsilon_\phi(t)$, as is true in most oscillators,

$$V_l(t) \approx K \cdot \varepsilon_\phi(t) \tag{3.10}$$

which is measured by the spectrum analyzer to get $S_\phi(f)$.

CHAPTER 4

UWB SYSTEM MODEL & COLORED JITTER MODEL

4.1 Chapter Overview

The single-user binary PPM system model to be used in the theoretical analysis and simulations of BER performance is described in this chapter. The binary PPM signaling and bit detection is extended to include timing jitters in the transmitter and receiver. The colored jitter phase noise model is also presented.

4.2 Binary PPM Signaling with Timing Jitter

The single-user signaling format for pulsed UWB using binary PPM is [2]

$$s(t,n) = \sum_{i=0}^{N_f-1} p(t - iT_f - b_n\delta), \tag{4.1}$$

where $s(t, n)$ is the transmitted signal representing the n^{th} bit, N_f is the number of pulses to represent one information bit, and T_f represents the pulse repetition time (time between pulses). The information of the n^{th} bit is encoded by delaying the pulse train by an additional $b_n\delta$, where $b_n \in \{0, 1\}$ is the n^{th} bit and δ is the PPM delay. Note that since we consider only the single-user scenario, the signal model in (4.1) ignores the use of time-hopping or direct-sequence codes. Many monocycle waveforms have been proposed in the literature. The popular Scholtz's monocycle [1] is used in this thesis. It is given by

$$p(t) = \left[1 - 4\pi\left(\frac{t}{T_n}\right)^2\right] e^{-2\pi\left[\frac{t}{T_n}\right]^2}, \tag{4.2}$$

where T_n denotes a time normalization factor, determining the monocycle's width. Figure 4.1 shows how the bit information is encoded onto the time positions of the Scholtz's monocycles.

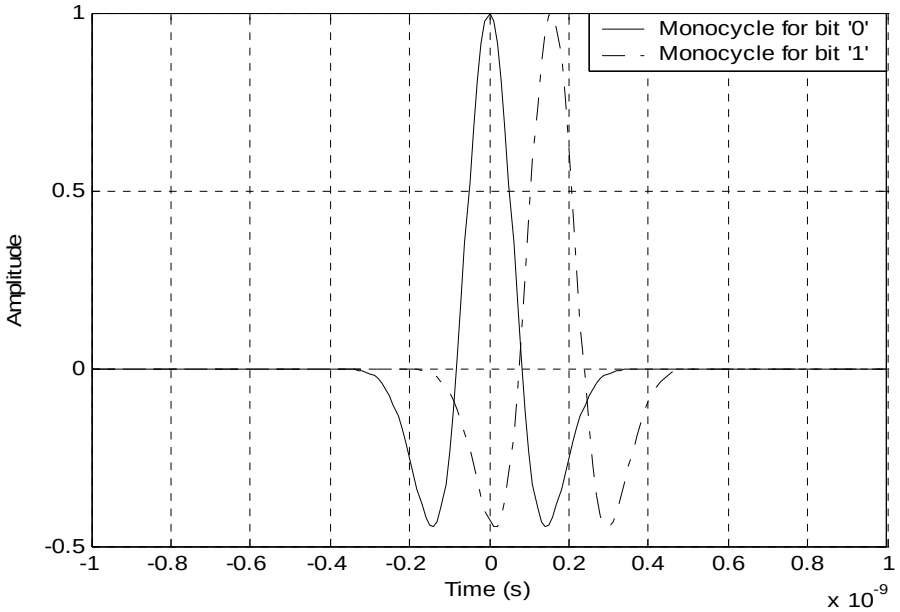

Figure 4.1: Bit information encoded onto Scholtz's monocycle positions

The pulse correlation function of $p(t)$ is the autocorrelation function of $p(t)$.

It is given in [20] as:

$$\begin{aligned} R_p(\tau) &= \int p(t)\,p(t+\tau)\,d\tau \\ &= \int p(t)\,p(t-\tau)\,d\tau \\ &= \left[1-4\pi\left(\frac{\tau}{T_n}\right)^2+\frac{4\pi^2}{3}\left(\frac{\tau}{T_n}\right)^4\right]e^{-\pi\left(\frac{\tau}{T_n}\right)^2} \end{aligned} \quad . \qquad (4.3)$$

Figure 4.2 shows the plot of $R_p(\tau)$.

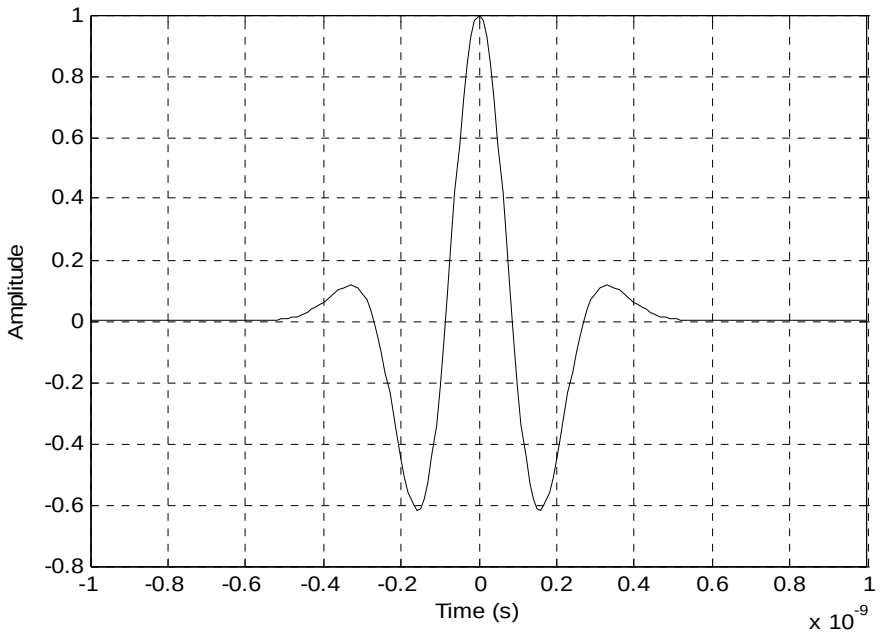

Figure 4.2: $R_p(\tau)$*, pulse correlation function of* p*(t)*

Since the aim of this thesis is to study the effect and compensation of timing jitter, a noiseless channel is assumed for simplicity. The received signal is thus

$$r(t,n) = \sum_{i=0}^{N_f-1} p(t - iT_f - b_n\delta - \varepsilon_i), \tag{4.4}$$

where e_i accounts for the total timing uncertainty due to the timing jitters in both the transmitter and the receiver as in [11]. In [11], e_i is assumed to be white Gaussian with zero mean. In this thesis, we relax this assumption to colored (correlated) timing jitter. We also assume perfect synchronization. Figure 4.3 illustrates how the timing jitters at each monocycle affect the monocycle position. The nominal frame position is at t = 0 ns, 4 ns and 8 ns.

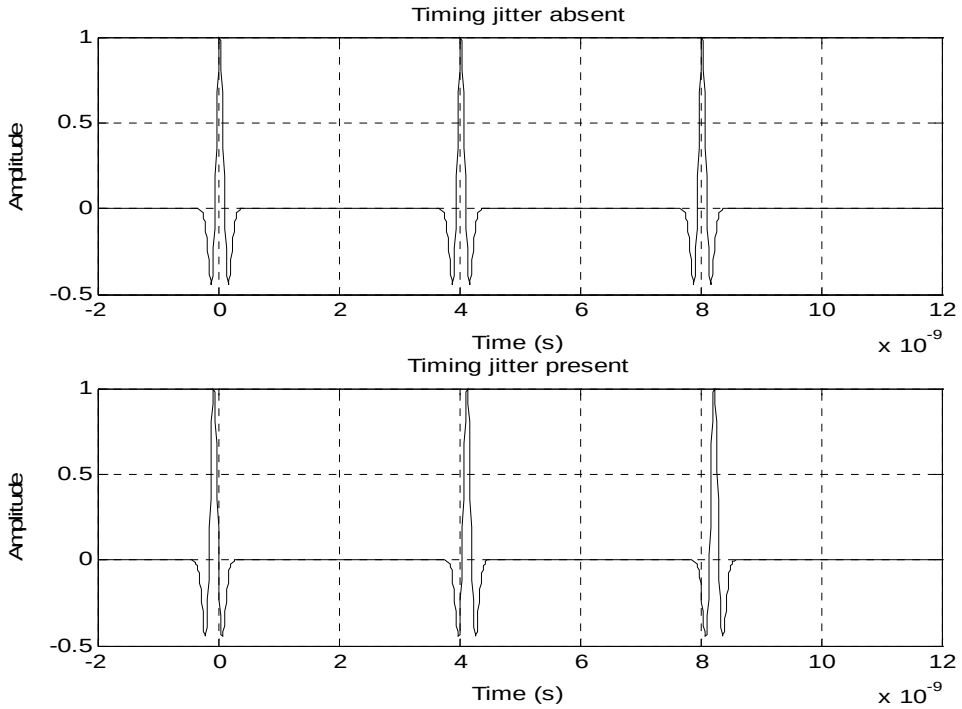

Figure 4.3: Effect of timing jitters on the monocycle positions

.

4.3 Binary PPM Bit Detection with Timing Jitter

The correlation template used for detection at the receiver is

$$v(t) = \sum_{i=0}^{N_f - 1} p(t - iT_f) - \sum_{i=0}^{N_f - 1} p(t - iT_f - \delta). \tag{4.5}$$

Figure 4.4 shows the correlation template *v(t)* for N_f = 1 pulse per bit. This is the waveform formed by subtracting the Scholtz's monocycle by its delayed version (delayed by *d*, the PPM delay).

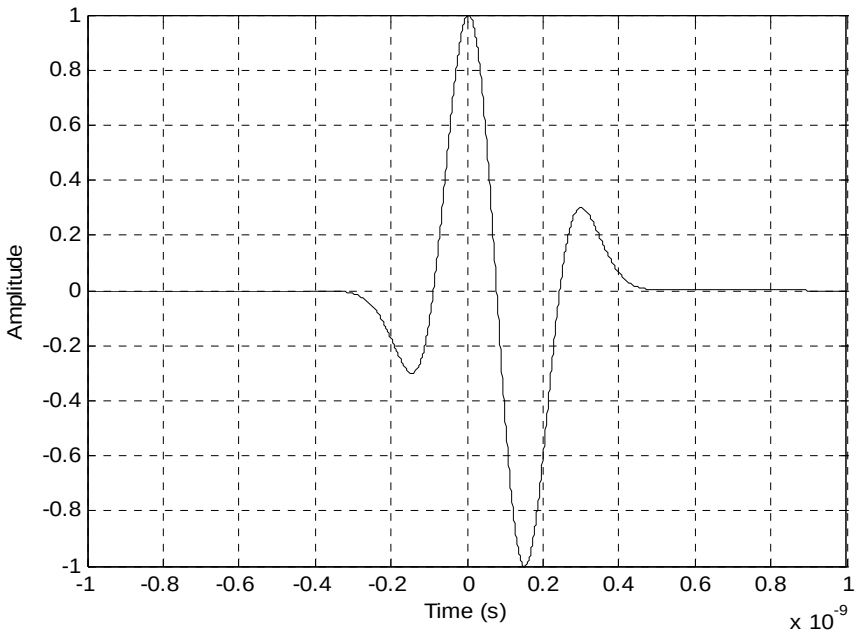

Figure 4.4: Binary PPM correlation template, v(t) for N_f = 1 pulse per bit.

Figure 4.5 shows the correlation template *v(t)* for N_f = 4 pulses per bit.

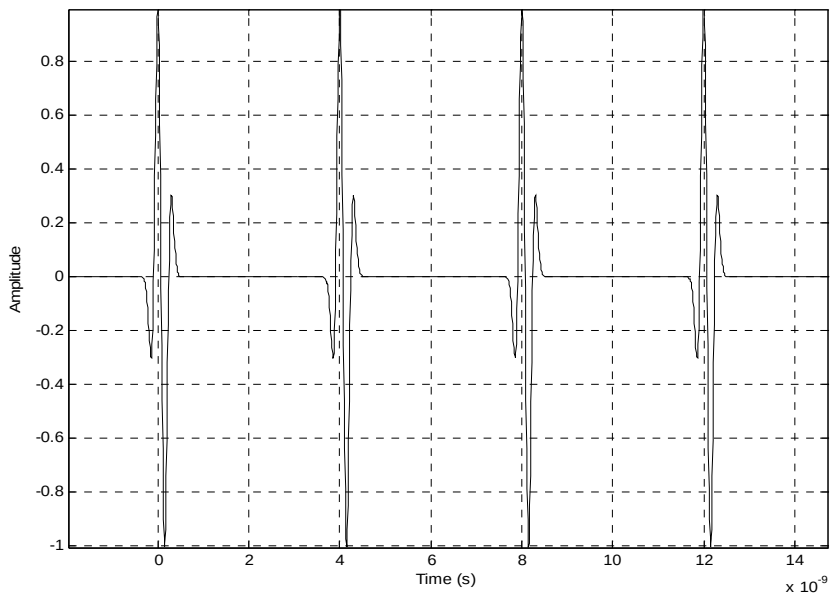

Figure 4.5: Binary PPM correlation template, v(t) for N_f = 4 pulses per bit.

The decision for the n^{th} bit is made in terms of the sign of the correlation of the received signal and the template:

$$\hat{b}_n = \begin{cases} 0 & \text{if} \quad d_n = \int r(t,n)v(t)dt > 0 \\ 1 & \text{if} \quad d_n = \int r(t,n)v(t)dt < 0 \end{cases}, \tag{4.6}$$

where d_n is the decision variable for the n^{th} bit and the integration is taken over the whole n^{th} bit's duration.

4.4 Colored Jitter Phase Noise Model

A VCO-PLL frequency synthesizer phase noise model [12] is adopted to model the colored phase jitter ε_ϕ:

$$S_\phi(f) = \frac{K}{f_L^{\,2} + f^2}, \tag{4.7}$$

where $S_\phi(f)$ is the power spectral density of the modeled phase jitter, f_L is the 3dB bandwidth, and K is a constant related to the jitter RMS value, ε_{rms} and f_L. The relationship between the phase jitter, ε_ϕ and the time jitter, ε is given in (3.3). Figure 4.4 shows the phase noise model for $f_L = 10^5 Hz$ and $\varepsilon_{rms} = 25 ps$

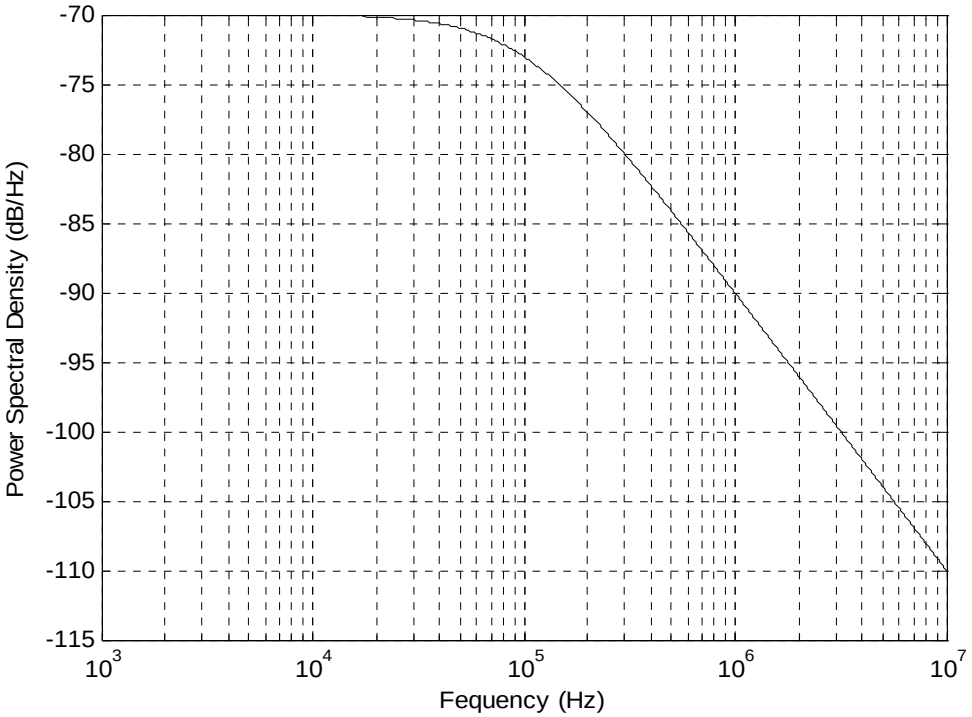

Figure 4.6: Colored Jitter Phase Noise Model

The colored timing jitter can be modeled as the output by filtering white Gaussian noise through a digital filter designed from the phase noise model in (4.7). Using bilinear transformation, it has the time-domain representation (to be derived later in Chapter 6)

$$\varepsilon_i = \frac{1}{1+\alpha}\left(x_i + x_{i-1} + (\alpha - 1)\varepsilon_{i-1}\right), \tag{4.8}$$

where x_i is white Gaussian with zero mean and variance σ_x^2. ε_i is the colored jitter with bandwidth f_L and RMS value ε_{rms}. α is a constant related to f_L and σ_x^2 is related to jitter RMS value ε_{rms} and f_L. α and σ_x^2 are adjusted to obtained colored jitter of a desired f_L and ε_{rms}. The relationships between the parameters σ_x^2, f_L, ε_{rms} and α will be clearly derived in Chapter 6.

CHAPTER 5

THEORETICAL ANALYSIS OF BER PERFORMANCE IN WHITE & COLORED TIMING JITTER

5.1 Chapter Overview

In this Chapter, a theoretical analysis of the effect of timing jitter on BER performance is presented. First the BER performance in white Gaussian timing jitter is derived. The effect of the jitter bandwidth on the BER performance is then analyzed theoretically. Finally, the upper and lower BER bounds for colored Gaussian timing jitter are obtained.

5.2 Effect of Timing Jitter in Bit Detection

The detection process essentially performs correlation between the received signal and the correlation template at the receiver. The pulse-template correlation function $R(\tau)$ is the cross-correlation function between the monocycle, $p(t)$, and the template, $v(t)$, which is the composite pulse formed from the difference between the two monocycles relatively delayed by the PPM delay δ. The pulse-template correlation function can be obtained in terms of the pulse correlation function in (4.3):

$$\begin{aligned} R(\tau) &= \int p(t)v(t+\tau)d\tau \\ &= \int p(t)\cdot\left[p(t+\tau)-p(t-\delta+\tau)\right]d\tau \\ &= \int p(t)\,p(t+\tau)d\tau - \int p(t)\,p(t-\delta+\tau)d\tau \end{aligned}$$

$$R(\tau) = R_p(\tau) - R_p(\tau - \delta). \tag{5.1}$$

The pulse-template correlation function $R(\tau)$ is plotted in Figure 5.1.

In the absence of timing jitter and with perfect synchronization and assuming a noiseless channel, according to the Pulse Position Modulation scheme described in (4.1), the pulse-template correlation value would have a maximum value of $R(0)$ and a minimum value of $R(\delta)$ if bit '0' and bit '1' are sent respectively. This can be clearly seen in Figure 5.1.

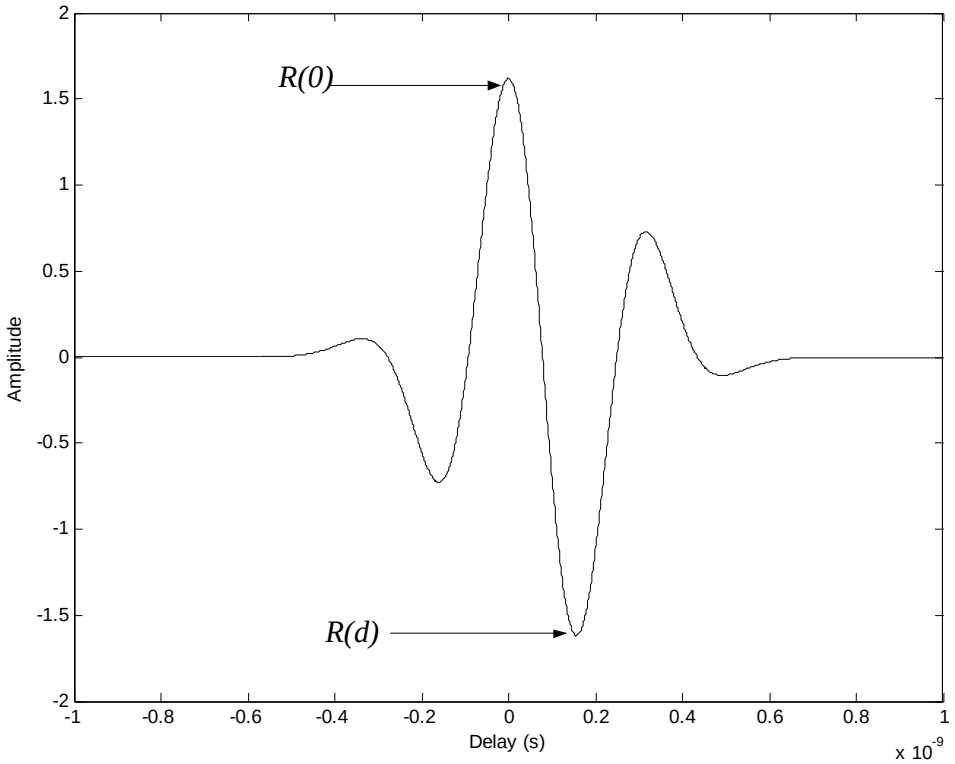

Figure 5.1. Pulse-template correlation function

In the presence of timing jitter, timing uncertainty causes random shifts in the time positioning of each monocycle. For example, if bit '0' is sent, the presence of jitter causes the pulse-template correlation for the ith pulse to assume a value of $R(e_i)$, where e_i is the timing jitter suffered by the i^{th} pulse, instead of the maximum $R(0)$. As a result, the pulse-template correlation value would be randomly distributed about its maximum $R(0)$ and its minimum $R(\delta)$ when bit '0' and '1' are sent respectively.

In accordance with the definitions for $r(t,n)$, $v(t)$, and d_n in (4.4), (4.5) and (4.6), and since ε_i is Guassian with zero mean, we further obtain

$$\begin{aligned}
d_n &= \int r(t,n)\cdot v(t)\partial t \\
&= \int \sum_{i=0}^{N_f-1} p(t-iT_f-b_n\delta-\varepsilon_i)\cdot\left[\sum_{i=0}^{N_f-1} p(t-iT_f)-\sum_{i=0}^{N_f-1} p(t-iT_f-\delta)\right]\cdot\partial t \\
&= \sum_{i=0}^{N_f-1}\int p(t-iT_f-b_n\delta-\varepsilon_i)\cdot\left[p(t-iT_f)-p(t-iT_f-\delta)\right]\cdot\partial t \\
&= \sum_{i=0}^{N_f-1}\int p(t-iT_f-b_n\delta-\varepsilon_i)\cdot p(t-iT_f)\cdot\partial t \\
&\quad -\sum_{i=0}^{N_f-1}\int p(t-iT_f-b_n\delta-\varepsilon_i)\cdot p(t-iT_f-\delta)\cdot\partial t \\
&= \sum_{i=0}^{N_f-1} R_p(\varepsilon_i+b_n\delta)-\sum_{i=0}^{N_f-1} R_p(\varepsilon_i+b_n\delta-\delta) \\
&= \sum_{i=0}^{N_f-1} R_p(\varepsilon_i+b_n\delta)-R_p(\varepsilon_i+b_n\delta-\delta) \\
&= \sum_{i=0}^{N_f-1} R(\varepsilon_i+b_n\delta)
\end{aligned} \tag{5.2}$$

where the third equality is due to the fact that successive pulses do not overlap (the duty cycle is very low at 1%) and the rest of the derivations follow from (5.1).

The optimal decision rule if bit '0' and '1' are sent with equal probability is simply (4.6). According to (4.6), an error will occur when the timing jitter value is large enough to cause the pulse correlation value to change sign (for example from positive to negative when bit '0' is in fact sent and from negative and positive when bit '1' is in fact sent).

5.3 BER Performance in White Timing Jitter

We now analyze the BER performance. For the binary case, the probability of error is given by

$$P_e = \sum_{i=0}^{1} P\left(\hat{b}_n \neq i \,|\, b_n = i\right) P\left(b_n = i\right). \tag{5.3}$$

From (4.6) and assuming bit '0' and '1' are sent with equal probability and due to the symmetry in the pulse-template correlation function $R(\tau)$, we have

$$\begin{aligned} P_e &= P\left(\hat{b}_n \neq 0 | b_n = 0\right) P\left(b_n = 0\right) + P\left(\hat{b}_n \neq 1 | b_n = 1\right) P\left(b_n = 1\right) \\ &= P\left(d_n < 0 | b_n = 0\right) \cdot \frac{1}{2} + P\left(d_n > 0 | b_n = 1\right) \cdot \frac{1}{2} \\ &= P\left(d_n < 0 | b_n = 0\right) \end{aligned} \quad .. \tag{5.4}$$

Substituting (5.2) into (5.4) yields

$$P_e = P\left(\sum_{i=0}^{N_f - 1} R(\varepsilon_i) < 0 \,|\, b_n = 0 \right). \tag{5.5}$$

$\sum_{i=0}^{N_f-1} R(\varepsilon_i)$ is the summation of N_f independently and identically distributed random variables. Since the number of pulses per bit, N_f, is typically large (>10), we may invoke the Central Limit Theorem and approximate $\sum_{i=0}^{N_f-1} R(\varepsilon_i)$ to have a Gaussian probability density function (PDF):

$$\sum_{i=0}^{N_f-1} R(\varepsilon_i) \sim N\left(N_f \cdot E\left[R(\varepsilon_i)\right],\ N_f \cdot Var\left[R(\varepsilon_i)\right]\right), \tag{5.6}$$

where

$$E\left[R(\varepsilon_i)\right] = \int_{-\infty}^{+\infty} R(\varepsilon_i) g(\varepsilon_i) d\varepsilon_i \tag{5.7}$$

$$Var\left[R(\varepsilon_i)\right] = E\left[R(\varepsilon_i)^2\right] - \left(E\left[R(\varepsilon_i)\right]\right)^2. \tag{5.8}$$

where $g(e_i)$ is the PDF of e_i which is Gaussian with zero mean and variance ε_{rms}^2. From the definition of $R(\tau)$ in (5.1) and $R_p(\tau)$ in (4.3)

$$E\left[R(\varepsilon_i)\right] = \int_{-\infty}^{+\infty} \left\{ \begin{array}{l} \left[1-4\pi\left(\frac{\varepsilon_i}{T_n}\right)^2 + \frac{4\pi^2}{3}\left(\frac{\varepsilon_i}{T_n}\right)^4\right] e^{-\pi\left(\frac{\varepsilon_i}{T_n}\right)^2} \\ -\left[1-4\pi\left(\frac{\varepsilon_i-\delta}{T_n}\right)^2 + \frac{4\pi^2}{3}\left(\frac{\varepsilon_i-\delta}{T_n}\right)^4\right] e^{-\pi\left(\frac{\varepsilon_i-\delta}{T_n}\right)^2} \end{array} \right\} \cdot \frac{1}{\varepsilon_{rms}\sqrt{2\pi}} e^{\left[-\frac{1}{2}\left(\frac{\varepsilon_i}{\varepsilon_{rms}}\right)^2\right]} \cdot d\varepsilon_i \tag{5.9}$$

and

$$E\left[\left(R(\varepsilon_i)\right)^2\right] = \int_{-\infty}^{+\infty} \left(R(\varepsilon_i)\right)^2 \cdot g(\varepsilon_i) \cdot d\varepsilon_i =$$

$$\int_{-\infty}^{+\infty} \left\{ \begin{array}{l} \left[1-4\pi\left(\frac{\varepsilon_i}{T_n}\right)^2 + \frac{4\pi^2}{3}\left(\frac{\varepsilon_i}{T_n}\right)^4\right] e^{-\pi\left(\frac{\varepsilon_i}{T_n}\right)^2} \\ -\left[1-4\pi\left(\frac{\varepsilon_i-\delta}{T_n}\right)^2 + \frac{4\pi^2}{3}\left(\frac{\varepsilon_i-\delta}{T_n}\right)^4\right] e^{-\pi\left(\frac{\varepsilon_i-\delta}{T_n}\right)^2} \end{array} \right\}^2 \cdot \frac{1}{\varepsilon_{rms}\sqrt{2\pi}} e^{\left[-\frac{1}{2}\left(\frac{\varepsilon_i}{\varepsilon_{rms}}\right)^2\right]} \cdot d\varepsilon_i$$

(5.10)

The $E\left[R(\varepsilon_i)\right]$ and $Var\left[R(\varepsilon_i)\right]$ for a particular jitter RMS value are evaluated by numerical integration of equation (5.9) and (5.10) using ***trapz*** function in MATLAB. Using these results, (5.5) can thus be further written as

$$P_e = Q\left(\frac{N_f \cdot E\left[R(\varepsilon_i)\right]}{\sqrt{N_f \cdot Var\left[R(\varepsilon_i)\right]}}\right), \tag{5.11}$$

where $Q(x) = \frac{1}{\sqrt{2\pi}} \int_x^\infty e^{-t^2/2} dt$.

The probability of error for a particular jitter RMS value can thus be deduced from the standardized normal variable cumulative distribution function table. This is tabulated in Table 5.1 for N_f = 100 pulses per bit.

ε_{rms} (ps)	$N_f \cdot E\left[R(\varepsilon_i)\right]$	$N_f \cdot Var\left[R(\varepsilon_i)\right]$	$\frac{0 - N_f \cdot E\left[R(\varepsilon_i)\right]}{\sqrt{N_f \cdot Var\left[R(\varepsilon_i)\right]}}$	$P_e = Q\left(\frac{N_f \cdot E\left[R(\varepsilon_i)\right]}{\sqrt{N_f \cdot Var\left[R(\varepsilon_i)\right]}}\right)$
10	158.8226	0.1768	-377.7465	0
30	137.1903	10.1205	-43.1244	0
50	104.0057	42.5378	-15.9466	0
70	71.0960	77.3633	-8.0831	0
80	57.0958	89.2228	-6.0446	0
90	45.2004	96.8191	-4.5937	2.2×10^{-6}
100	35.3967	100.8685	-3.5244	2.12×10^{-4}
110	27.5047	102.3046	-2.7193	3.27×10^{-3}
120	21.2633	101.9717	-2.1057	1.762×10^{-2}
130	16.3912	100.5179	-1.6349	5.104×10^{-2}
140	12.6229	98.3969	-1.2725	1.016×10^{-1}
150	9.7259	95.9079	-0.9931	1.603×10^{-1}
160	7.5066	93.2410	-0.7774	2.185×10^{-1}
170	5.8092	90.5138	-0.6106	2.707×10^{-1}
180	4.5107	87.7975	-0.4814	3.151×10^{-1}

Table 5.1:Tabulation of Probability of Error in White Gaussian Jitter, for N_f = 100 pulses per bit

5.4 Effect of Colored Jitter Bandwidths on BER Performance

For the colored jitter case, unlike the white jitter case, the BER expression in equation (5.5),

$$P_e = P\left(\sum_{i=0}^{N_f-1} R(\varepsilon_i) < 0 \,|\, b_n = 0 \right)$$

cannot be expressed in simpler terms because the successive $R(\varepsilon_i)$ are correlated and not independent. Hence the Central Limit Theorem cannot be used to approximate the distribution of the sum of $R(\varepsilon_i)$ terms. Nonetheless, some analysis is possible to derive an upper and lower bound for the BER performance in colored timing jitter.

For colored jitter, as the jitter bandwidth f_L decreases, successive jitter samples become more correlated. Successive pulse-template correlation values, $R(e_i)$, within the same bit also become more correlated. Consider the sum of N_f independently Gaussian distributed random variables x_i (i = 0, 1, …, N_f – 1) with mean μ and variance σ^2 in the probability expression:

$$P\left(\sum_{i=0}^{N_f-1} x_i < \gamma \right), \tag{5.12}$$

where *?* is a constant. Obviously, the PDF of $\sum_{i=0}^{N_f-1} x_i$ is

$$N(N_f \mu,\ N_f \sigma^2)\,. \tag{5.13}$$

On the other hand, if the random variables x_i (i = 0, 1, …, N_f – 1) are completely dependent and equal to each other (i.e., $x_0 = x_1 = \ldots = x_{N_f-1} = x$), (5.12) becomes

$$P\left(N_f x < \gamma \right) \tag{5.14}$$

with a PDF of

$$N(N_f \mu, N_f^2 \sigma^2). \tag{5.15}$$

By considering the areas (see Figure 5.2) under the two Gaussian PDFs in (5.13) and (5.15), we can therefore deduce

$$P\left(\sum_{i=0}^{N_f-1} x_i < \gamma\right) < P\left(N_f x < \gamma\right) \tag{5.16}$$

if both the left hand side and the right hand side are smaller than 0.5. This is true for probability of bit error.

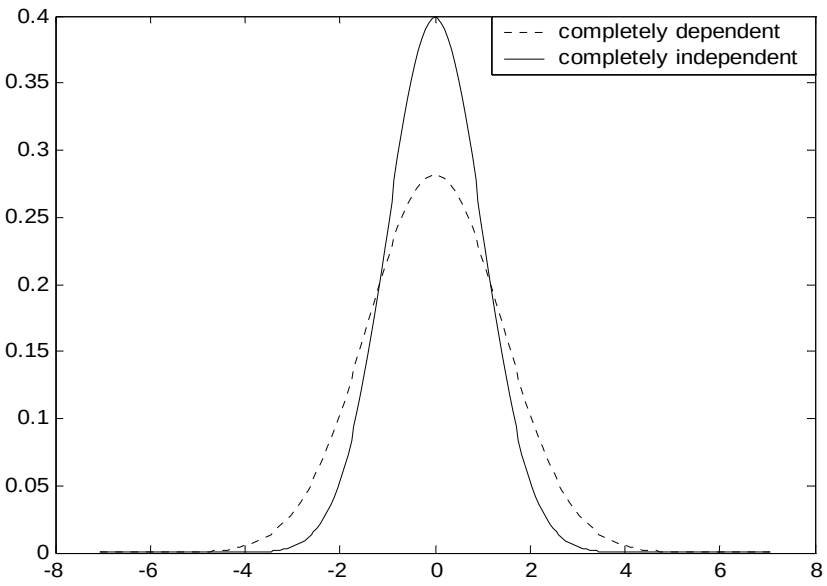

Figure 5.2: Two Gaussian PDFs of the same mean but different variance

As f_L decreases, successive values of e_i become more correlated, which in turn leads to successive values of $R(e_i)$ become more correlated. If the non-guassian probability distribution function of $R(e_i)$ behaves like the normal distribution described above, we

can conclude from (5.5) and (5.16) that the BER increases as f_L decreases. In section 7.4, the simulation results show that this is true.

5.5 Upper and Lower Bounds for BER Performance in Colored Jitter

It is clear that the BER performance in colored jitters of any f_L for $N_f > 1$ pulses per bit is lower bounded by that in white jitters for the same N_f pulses per bit, since successive jitter values are independent for white jitter. The theoretical upper bound can be obtained by assuming that every jitter value during one bit duration is the same or fully dependent (i.e., $\varepsilon_0 = \varepsilon_1 = \cdots = \varepsilon_{N_f-1} = \varepsilon$). For this case, the BER expression in (5.5) reduces to

$$\begin{aligned} P_e &= P\left(N_f R(\varepsilon) < 0 \,|\, b_n = 0\right) \\ &= P\left(R(\varepsilon) < 0 \,|\, b_n = 0\right) \\ &= Q\left(\frac{E\left[R(\varepsilon)\right]}{\sqrt{Var\left[R(\varepsilon)\right]}}\right), \end{aligned} \tag{5.17}$$

which is the probability of error in (5.11) for the case of single pulse per bit.

Figure 5.3 shows the upper and lower bounds for the BER performance under colored timing jitter for N_f = 100 pulses per bit. The upper bound is the derived BER performance in white timing jitter for N_f = 1 pulse per bit while the lower bound is the derived BER performance in white timing jitter for N_f = 100 pulses per bit.

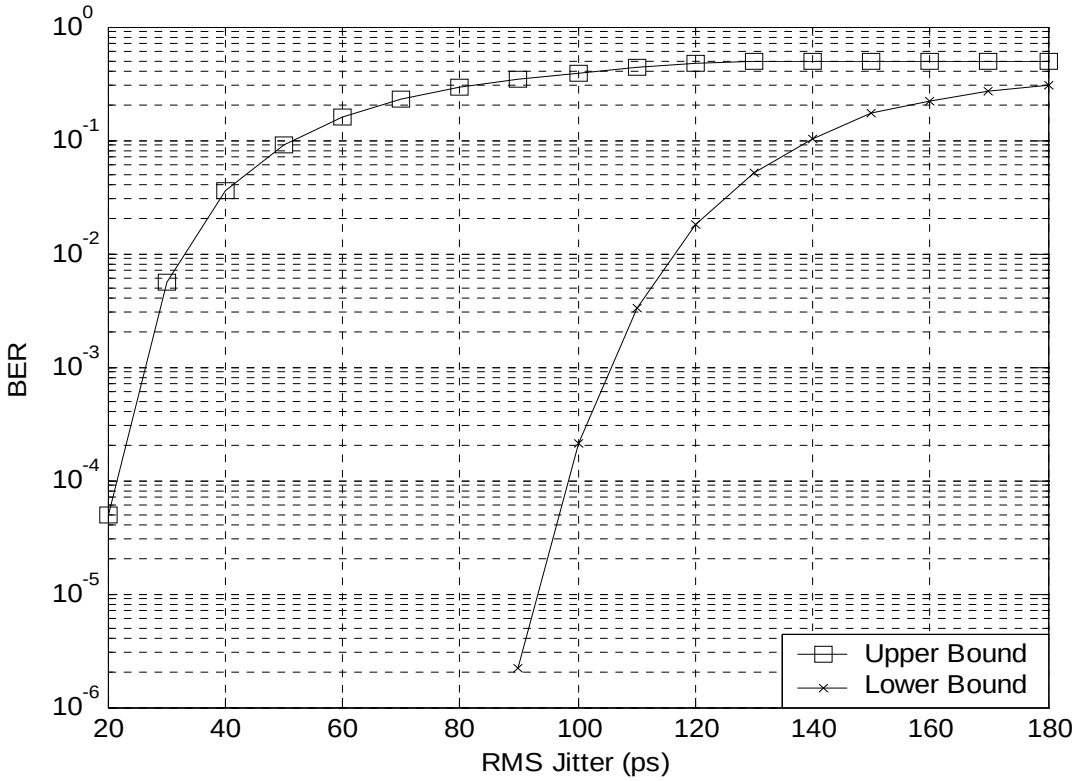

Figure 5.3: Upper and lower bound for BER performance in colored timing jitter for N_f = 100 pulses per bit.

CHAPTER 6

FILTER DESIGN & GENERATION OF COLORED JITTER

6.1 Chapter Overview

This chapter presents the filter design of the desired digital filter by bilinear transformation, followed by a description of how the colored jitter used in the simulations is generated, and finally verifies that the generated colored jitter indeed has a power spectrum agreeing with the colored jitter phase noise model adopted in Chapter 4.

6.2 Digital Filter Design (by Bilinear Transformation)

The VCO-PLL frequency synthesizer phase noise model adopted [12] is:

$$S_\phi(f) = \frac{K}{f_L{}^2 + f^2} \tag{6.1}$$

where $S_\phi(f)$ is the PSD of ε_ϕ, the phase jitter in radian, f_L is the loop 3dB bandwidth and *K* is a constant which can be determined from the in-band noise floor observed from a spectrum analyzer measurement.

The in-band noise floor, N_{floor} in *dB/Hz*, is related to *K* and f_L:

$$N_{floor} = 10\lg\left[S_\phi(f)|_{f=0}\right] = 10\cdot\lg\left[\frac{K}{f_L{}^2}\right] \tag{6.2}$$

Alternatively,

$$K = f_L^{\,2} 10^{\frac{N_{floor}}{10}}$$

so the phase noise model in terms of f_L and N_{floor}:

$$S_\phi(f) = \frac{10^{\frac{N_{floor}}{10}}}{1+(f/f_L)^2} \tag{6.3}$$

Figure 6.1 shows the phase noise model for $f_L = 10^5 Hz$ and $N_{floor} = -70 dB/Hz$

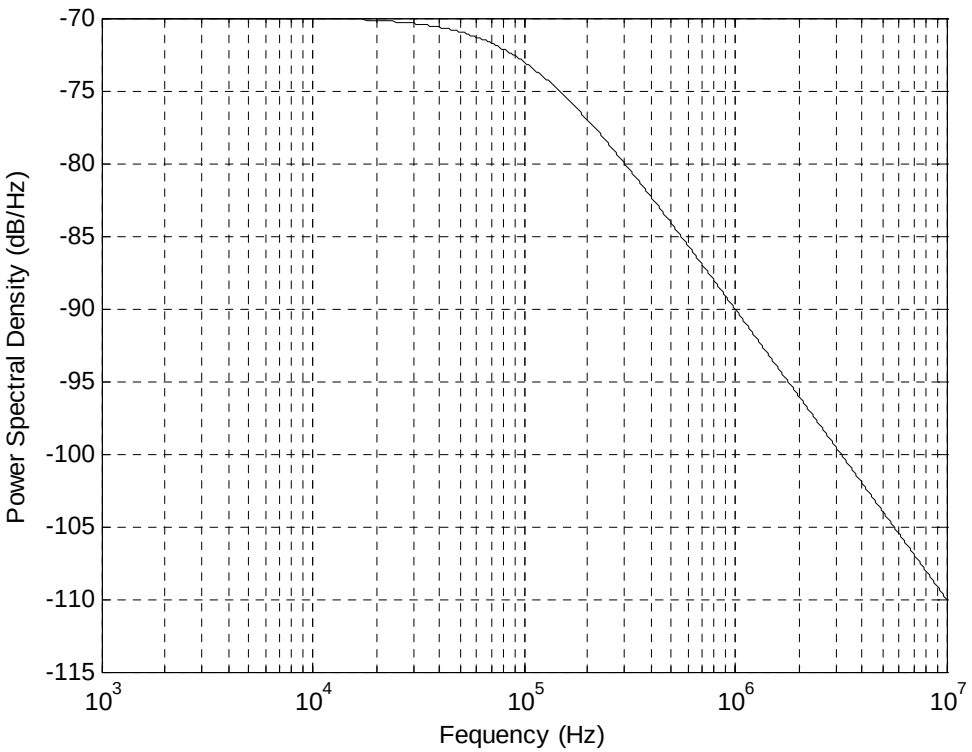

Figure 6.1: Phase Noise Model

Consider an analogue filter with transfer function H(s) with unity dc gain:

$$H(s) = \frac{2\pi f_L}{2\pi f_L + s} \tag{6.4}$$

The square of magnitude response of *H(s)* fits the phase noise model:

$$|H(s)|^2 = \left|\frac{2\pi f_L}{2\pi f_L + jw}\right|^2 = \frac{{f_L}^2}{{f_L}^2 + f^2} = |H(f)|^2 \tag{6.5}$$

It also has 3dB bandwidth at f_L. Figure 5.2 shows the bode magnitude plot for *H(s)* when $f_L = 10^5 Hz$.

(Note that the horizontal axis is in radian/s)

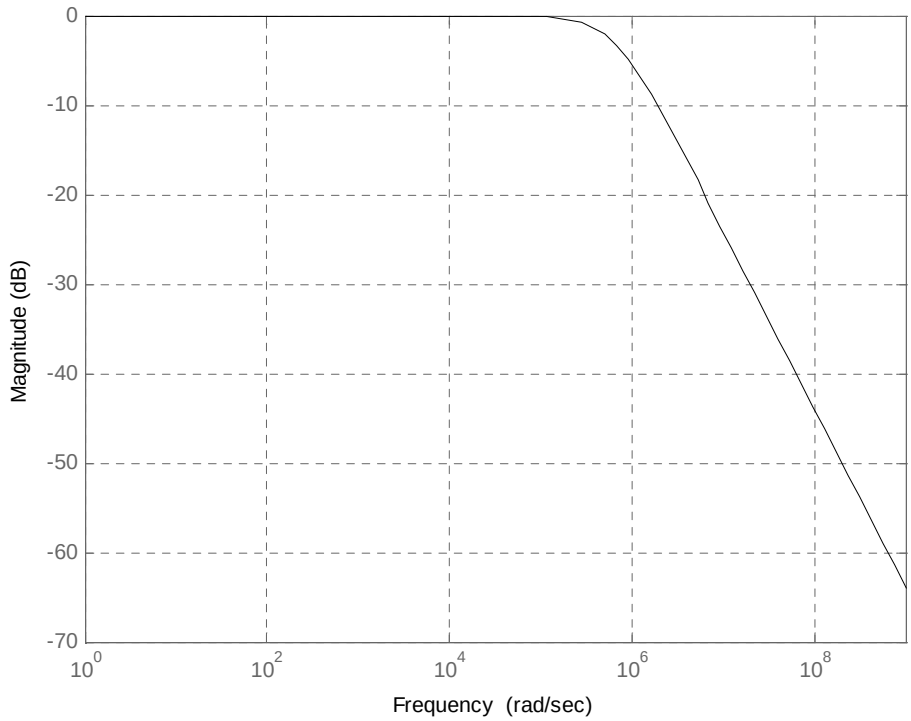

Figure 6.2: Bode Magnitude Plot of Analogue Filter H(s)

The bilinear transformation method to design a digital filter from a known analogue filter maps the variable *s* to *z* in the filter transfer function according to the following:

$$s \to A\frac{1-z^{-1}}{1+z^{-1}} \tag{6.6}$$

where *A* is a constant defined by

$$A = \frac{\Omega}{\tan\left(\frac{w}{2}\right)} \tag{6.7}$$

where Ω is the analogue angular frequency to be matched to the digital angular frequency, *w*.

Matching at the 3 dB frequency,

$$\Omega = 2\pi f_L \tag{6.8}$$

$$w = 2\pi\frac{f}{f_s} = 2\pi\frac{f_L}{f_s}, \tag{6.9}$$

where f_s is the sampling frequency of the filter.

So (6.7) becomes

$$A = \frac{2\pi f_L}{\tan\left(\frac{\pi f_L}{f_s}\right)} \tag{6.10}$$

Mapping the analogue filter transfer function in (6.4) using equation (6.6), the digital filter transfer function designed by Bilinear Transformation is

$$H(z) = \frac{z+1}{(1+\frac{A}{2\pi f_L})z + (1-\frac{A}{2\pi f_L})} \tag{6.11}$$

Figure 6.3 shows the bode magnitude plot for the digital filter *H(z)* when $f_L = 10^5 Hz$.

(Note that the horizontal axis is in radian/s)

It agrees with the bode magnitude plot for the analogue filter *H(s)*.

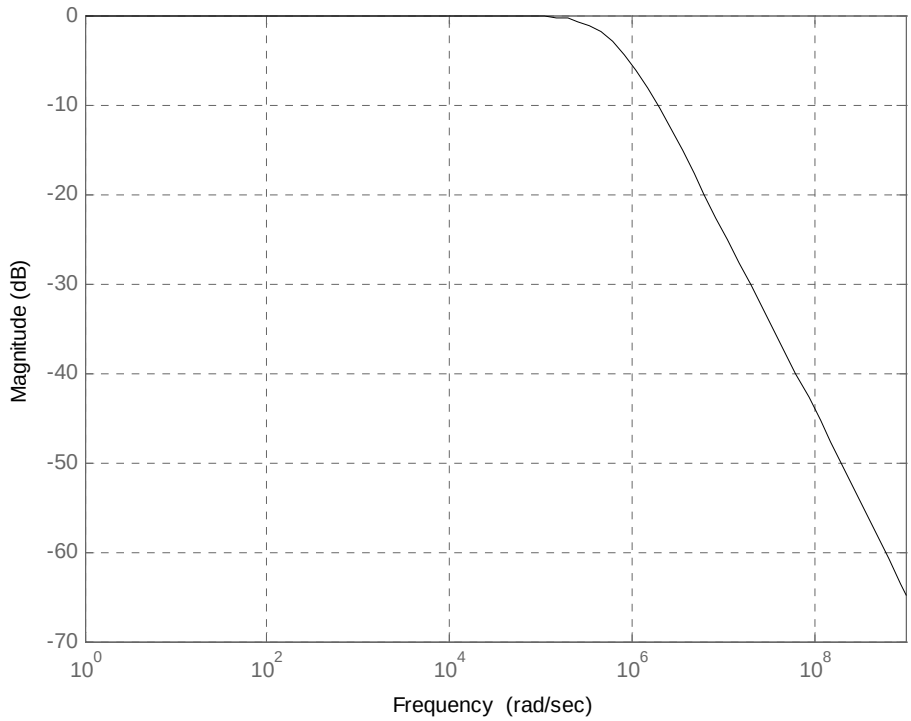

Figure 6.3: Bode Magnitude Plot of Digital Filter H(z)

6.3 Time-Domain Representation of the Phase Noise Model

The colored Gaussian jitter used in our simulations is obtained by filtering white noise with the designed digital filter. From (6.10 and 6.11), the filter has transfer function

$$H(z) = \frac{z+1}{(1+\frac{A}{2\pi f_L})z + (1-\frac{A}{2\pi f_L})}$$

where $A = \frac{2\pi f_L}{\tan(\frac{\pi f_L}{f_s})}$

and f_s is the sampling frequency of the filter and f_L is the 3dB bandwidth.

Let the input to the filter, w be white Gaussian noise and ε_ϕ be the output colored Gaussian noise (which is the colored phase jitter). Thus

$$H(z) = \frac{\varepsilon_\phi(z)}{w(z)} = \frac{z+1}{(1+\frac{A}{2\pi f_L})z + (1-\frac{A}{2\pi f_L})}. \tag{6.12}$$

After cross-multiplying,

$$(1+\frac{A}{2\pi f_L})z \cdot \varepsilon_\phi(z) + (1-\frac{A}{2\pi f_L}) \cdot \varepsilon_\phi(z) = z \cdot w(z) + w(z). \tag{6.13}$$

After performing the inverse Z-Transform

$$\varepsilon_\phi(n+1) = \frac{1}{1+\frac{A}{2\pi f_L}} \cdot \left\{ w(n+1) + w(n) - \left(1-\frac{A}{2\pi f_L}\right)\varepsilon_\phi(n) \right\} \tag{6.14}$$

which is equivalent to

$$\varepsilon_\phi(n) = \frac{1}{1+\frac{A}{2\pi f_L}} \cdot \left\{ w(n) + w(n-1) - \left(1-\frac{A}{2\pi f_L}\right)\varepsilon_\phi(n-1) \right\} \tag{6.15}$$

Define the constant a = $\frac{A}{2\pi f_L} = \frac{1}{\tan(\frac{\pi f_L}{f_s})}$. (6.16)

Thus the relationship between successive phase jitter samples is

$$\varepsilon_\phi(n) = \frac{1}{1+\alpha} \cdot \left\{ w(n) + w(n-1) + (\alpha - 1)\varepsilon_\phi(n-1) \right\}. \quad (6.17)$$

Expressing (6.17) in terms of time jitter ε instead of phase jitter ε_ϕ, knowing the relationship between them from (3.3):

$$\varepsilon(n) = \frac{1}{1+\alpha} \cdot \left\{ \frac{1}{2\pi f_c} w(n) + \frac{1}{2\pi f_c} w(n-1) + (\alpha - 1)\varepsilon(n-1) \right\} \quad (6.18)$$

where f_c is the nominal clock oscillator frequency. Equivalently we have

$$\varepsilon(n) = \frac{1}{1+\alpha} \cdot \left\{ x(n) + x(n-1) + (\alpha - 1)\varepsilon(n-1) \right\} \quad (6.19)$$

where $x = \frac{1}{2\pi f_c} w$.

x is also zero mean white Gaussian noise with a different variance from *w*. The required variance σ_w^2 of the white Gaussian noise to be filtered to generate time jitter ε, of a desired jitter bandwidth f_L and jitter RMS value ε_{rms} is derived in the next section.

6.4 Generation of Colored Jitter

By filtering white Gaussian noise, *w*, of appropriate power, σ_w^2 using the designed digital filter, the generated colored phase jitter ε_ϕ, will have a PSD in agreement with the colored jitter phase noise model adopted. From the colored phase jitter, the colored time jitter ε is obtained having jitter bandwidth f_L and jitter RMS value ε_{rms}. The relationship between ε_{rms} and σ_w^2 is derived below for a desired f_L.

The power spectral density of the white noise with power σ_w^2, assuming it is band limited at $\pm\frac{f_s}{2}$ is

$$S_w(f) = \frac{\sigma_w^2}{f_s}. \tag{6.20}$$

From (6.5), the square of the magnitude response of the designed filter is

$$|H(f)|^2 = \frac{{f_L}^2}{{f_L}^2 + f^2}$$

The phase jitter mean square power, $\varepsilon_{\phi,rms}^2$ can be approximated by

$$\begin{aligned}
\varepsilon_{\phi,rms}^2 &= \int_{-\infty}^{+\infty} |H(f)|^2 S_w(f) df \\
&= \int_{-\frac{f_s}{2}}^{\frac{f_s}{2}} \frac{f_L^2}{f_L^2 + f^2} \cdot \frac{\sigma_w^2}{f_s} df \\
&= \frac{f_L \sigma_w^2}{f_s} \cdot \int_{-\frac{f_s}{2}}^{\frac{f_s}{2}} \frac{f_L}{f_L^2 + f^2} df
\end{aligned}$$

$$\begin{aligned}\varepsilon_{\phi,rms}^2 &= \frac{f_L\sigma_w^2}{f_s}\left[\tan^{-1}\left(\frac{f_s}{2f_L}\right)-\tan^{-1}\left(\frac{-f_s}{2f_L}\right)\right]\\ &\approx \frac{f_L\sigma_w^2}{f_s}\left[\frac{\pi}{2}-\left(-\frac{\pi}{2}\right)\right]\\ &= \frac{\pi f_L}{f_s}\sigma_w^2\end{aligned} \quad . \tag{6.21}$$

The approximation holds if f_s is much greater than f_L, which is true in this thesis.

Thus from the relationship between the phase jitter in units of radian, ε_ϕ, and the time jitter in units of second, ε, in (3.3),

$$\begin{aligned}\varepsilon_{rms}^2 &= \left(\frac{\varepsilon_{\phi,rms}}{2\pi f_c}\right)^2\\ &= \frac{f_L\sigma_w^2}{4\pi f_c^{\,2} f_s}\end{aligned} \tag{6.22}$$

where f_c is the nominal frequency of the clock. Alternatively,

$$\sigma_w^2 = \frac{4\pi f_c^{\,2} f_s}{f_L}\varepsilon_{rms}^2 . \tag{6.23}$$

The ***filter*** function in MATLAB is used to filter a white Gaussian data sequence of zero mean and variance σ_w^2 using the digital filter derived in (6.11). The output from the filter is colored phase jitter of bandwidth f_L and RMS value $\varepsilon_{\phi,rms}$. From this and (3.3), the colored time jitter, ε, of bandwidth f_L and RMS value ε_{rms} is obtained. The equivalent equation describing the filtering operation was derived in (6.19) as

$$\varepsilon(n) = \frac{1}{1+\alpha}\cdot\left\{x(n)+x(n-1)+(\alpha-1)\varepsilon(n-1)\right\}$$

where $x = \frac{1}{2\pi f_c}w$

Thus from (6.18) and (6.23), the variance of x in (6.19) is

$$\sigma_x^2 = \frac{f_s}{\pi f_L}\varepsilon_{rms}^2 \tag{6.24}$$

In summary, to generate colored timing jitter of a particular jitter bandwidth f_L and a particular jitter RMS value ε_{rms}, first set the filter coefficient to be *A* in accordance with (6.10) to get the desired jitter bandwidth f_L and then set the variance of the white noise input to be σ_w^2 in accordance with (6.23) to get the desired jitter RMS value ε_{rms}.

Figure 6.4 shows a realization of the colored timing jitter waveform (in second) generated when $f_L = 10^5\,Hz$ and $\varepsilon_{rms} = 25\,ps$.

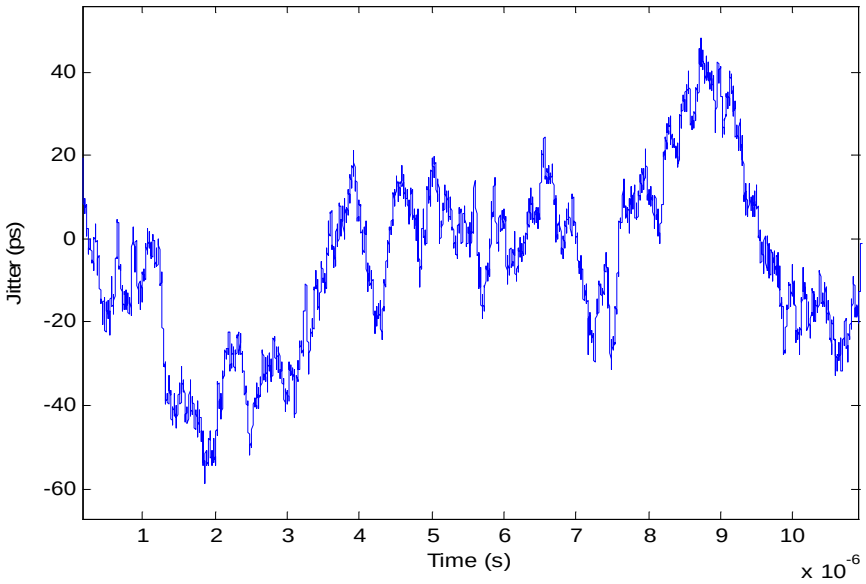

Figure 6.4: A realization of generated colored timing jitter, f_l = 1e5 Hz and $\varepsilon_{rms} = 25\,ps$

As f_L increases, the jitter waveform becomes more 'busy'. Figure 6.5 shows the colored jitter at a higher f_L of 10^6 Hz for the same $\varepsilon_{rms} = 25\,ps$.

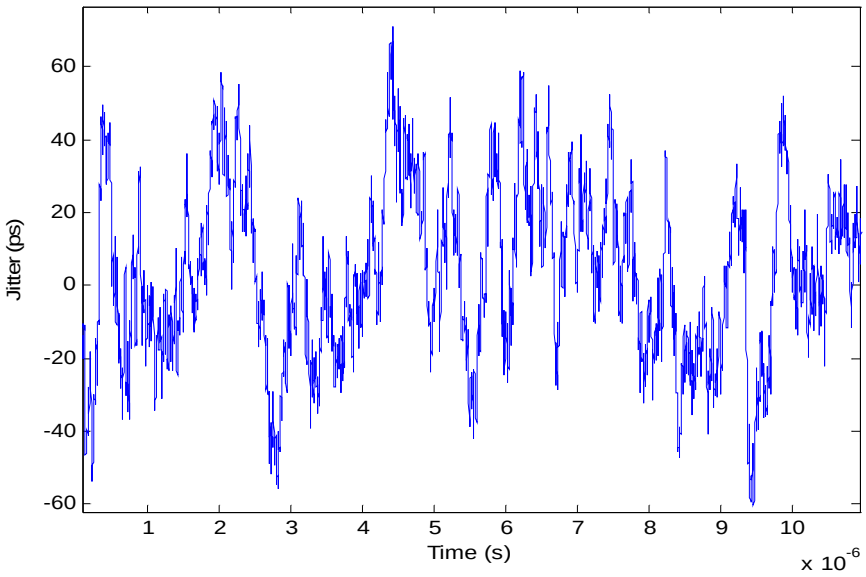

Figure 6.5: A realization of generated colored timing jitter, $f_l = 10^6$ Hz and $\varepsilon_{rms} = 25\,ps$

6.5 Verifying the Generated Colored Jitter

The MATLAB function ***pmcov*** uses an autoregressive spectral estimation algorithm to estimate the PSD of a data sequence assumed to be the output of a linear system driven by white noise. Using ***pmcov***, the bandwidth and power of the generated colored phase jitter may be checked for agreement with the adopted phase noise model.

Figure 6.6 shows the PSD estimate of the colored phase jitter associated with Figure 6.4, where $f_l = 10^6$ Hz and $\varepsilon_{rms} = 25$ps. From (6.2), (6.20) and (6.22), for these values of f_l and ε_{rms}, the inband noise floor is obtained at -70 dB/Hz. Comparing Figure 6.6 with Figure 6.1, indeed the generated colored jitter has a PSD agreeing with the adopted phase noise model.

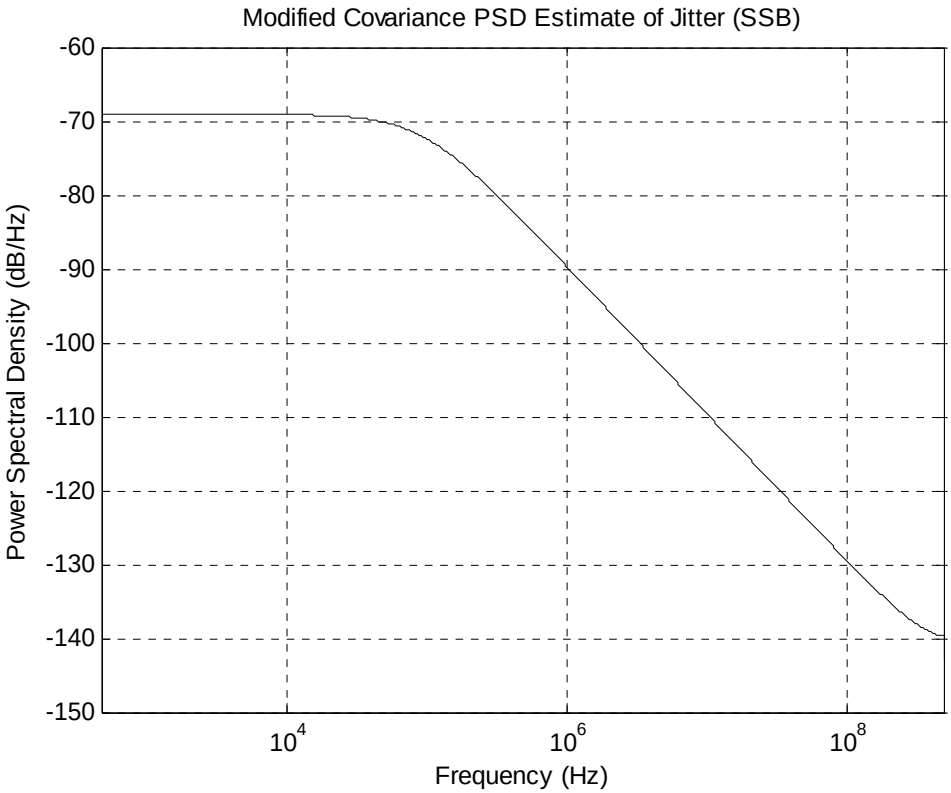

Figure 6.6: Estimated PSD of Generated Colored Jitter

CHAPTER 7

SIMULATION SETUP & RESULTS

7.1 Chapter Overview

In this chapter, the BER performance of a binary Pulse Position Modulation (PPM) single-user UWB communication system subjected to both white and colored clock timing jitter is investigated via simulations. The results are presented after the simulation setup is described and key parameters are chosen.

7.2 Simulation Setup and Parameters

The monocycle used is the Scholtz's monocycle which was also used in [11]:

$$p(t) = \left[1 - 4\pi\left(\frac{t}{T_n}\right)^2\right] e^{-2\pi\left[\frac{t}{T_n}\right]^2} \tag{7.1}$$

where the parameter T_n is chosen to be 0.29ns satisfying the relation $\int_{-\infty}^{\infty} p(t)dt = 0$. The resulting monocycle has a very narrow impulse width of less than 1 ns and is plotted in Figure 7.1. The frame interval, T_f, is chosen to be 100ns to obtain a typical 1% duty cycle and the number of chips per bit, N_f, is chosen to be 100 pulses/bit. The binary PPM modulation parameter, δ, is chosen to be 156ps to maximize (4.3).

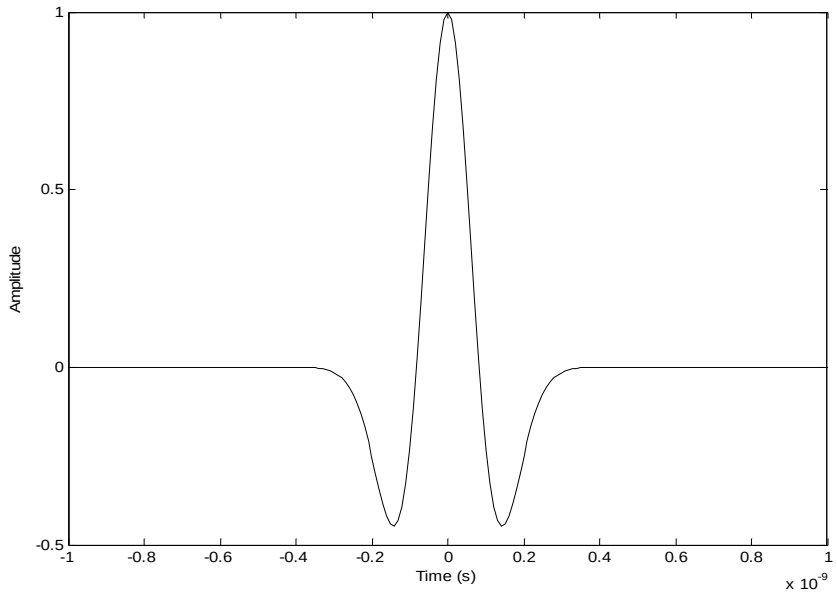

Figure 7.1: Scholtz Monocycle with T_n = 0.29ns

In the white jitter case the timing jitter e_i is sampled from the zero mean Gaussian distribution with standard deviation equal to the jitter RMS value, e_{rms}. Each successive e_i should be statistically independent. The MATLAB function ***Randn*** is used to generate the e_i required in simulation. For each jitter RMS value, the total number of trials, *L*, and the number of errors made, *M*, are recorded and the bit error rate is estimated as *M/L*. In the colored jitter case, e_i is taken from the output of filtering the white Gaussian samples of zero mean and appropriate variance with the designed digital filter as described in Chapter 6.

7.3 Statistical Validity

In the simulations, the probability of transmitting bit ‘0’ is chosen to be the same of transmitting bit ‘1’ and adjacent bits transmitted in adjacent time slots are statistically independent.

Statistical validity of the simulated results has been considered. Suppose that in a particular simulation run, L bits are being simulated and the receiver makes M erroneous decisions out of the total L bits. Then if L is large enough, the average probability of bit error (bit error rate) will approximate M/L according to probability theory. If L is 100 times the reciprocal of the bit error rate, the resulting root mean-square measurement error is less than 10 percent [21]. To achieve statistical reliability in the simulation results, L is adjusted accordingly such that it is at least 100 times the reciprocal of the bit error rate obtained.

7.4 BER Performance in White Gaussian Jitter

Figure 7.2 shows the simulated BER performance in white Gaussian jitter for N_f = 100 pulses per bit plotted together with the theoretical curve for comparison. Figure 7.3 shows the simulated BER performance for N_f = 1 pulse per bit plotted together with the theoretical curve for comparison. Clearly the simulation result agrees very well with the analytical derivations in Chapter 5.

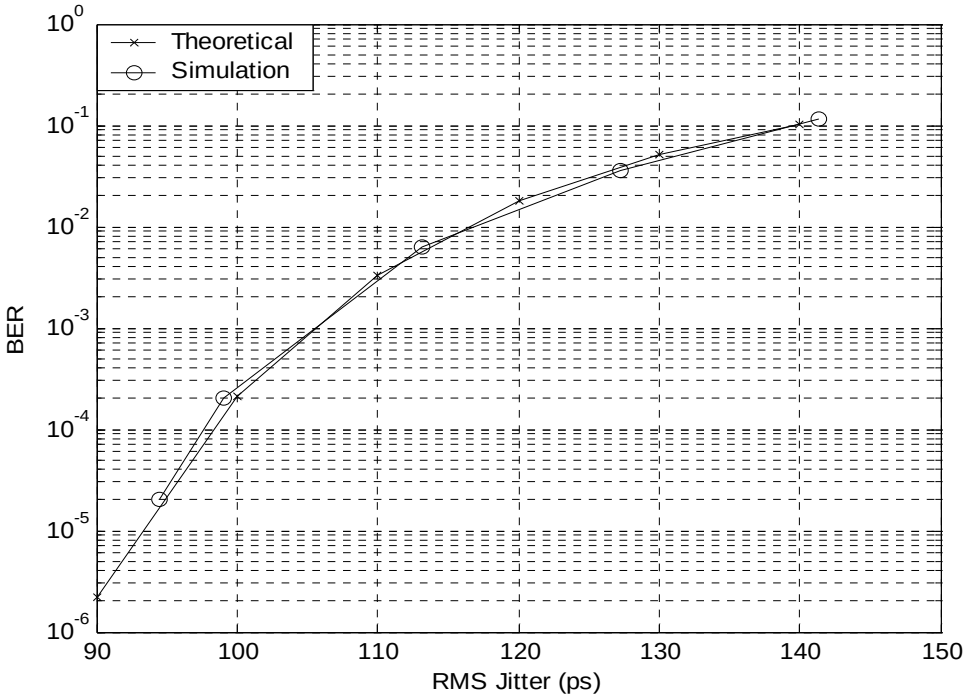

Figure 7.2: BER Performance in White Gaussian Jitter for 100 pulses per bit

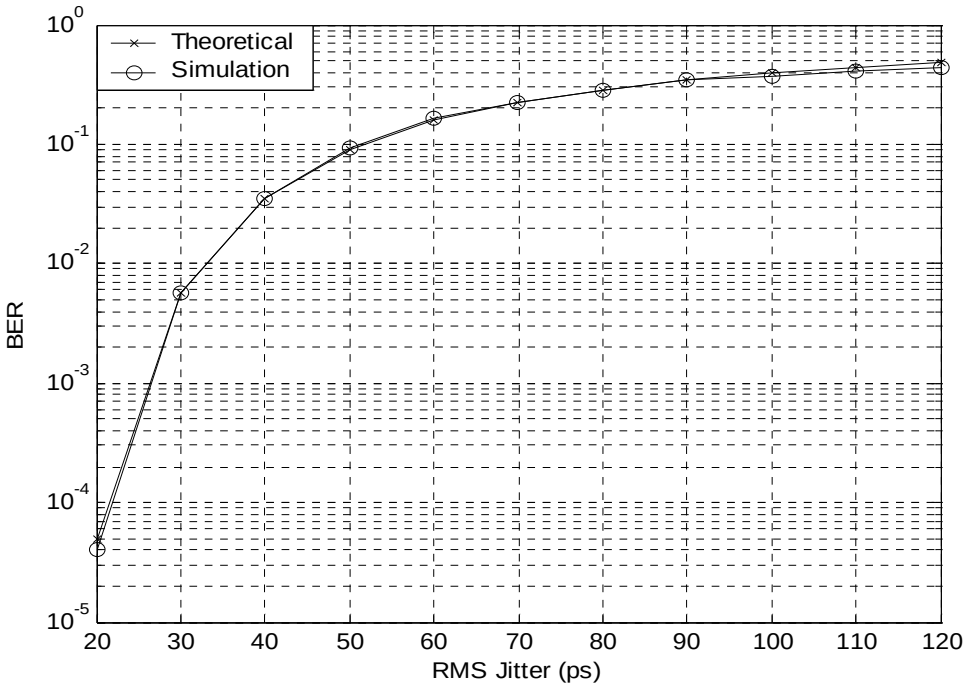

Figure 7.3: BER Performance in White Gaussian Jitter for 1 pulse per bit

7.5 BER performance in Colored Gaussian Jitter

Figure 7.4 shows the BER performance in colored jitters versus the jitter RMS values (from 0 to 180ps) for various jitter bandwidth (10^4 to 10^7 Hz). As a comparison, the theoretical upper and lower bounds derived in Chapter 5 are also plotted. It can be seen from the figure that the BER performance degrades significantly as the jitter bandwidth f_L decreases, as predicted by the theoretical analysis. A jitter RMS value of 105ps for white jitter results in a BER of 10^{-3}, while for colored jitter with a 3 dB bandwidth of 10^5 Hz, a significantly smaller jitter RMS value of 25ps results in the same BER. The BER curves are also within the derived bounds, confirming the theoretical analysis.

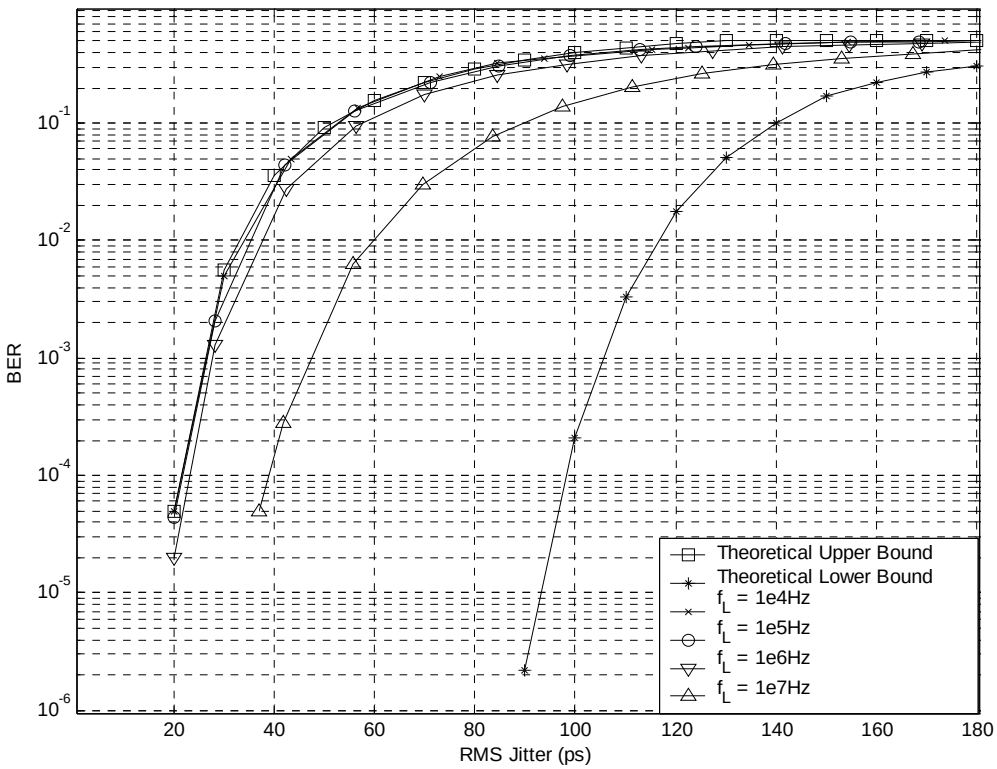

Figure 7.4: BER Performance in Colored Gaussian Jitter for N_f = 100 pulses per bit

CHAPTER 8

JITTER COMPENSATION ALGORITHM

8.1 Chapter Overview

In this chapter, the motivation and approach in the design of the proposed jitter compensation algorithm is presented, followed by a detailed discussion on the three components of the algorithm namely: Jitter Tracker, Jitter Estimator and a Maximal-Likelihood (ML) decision rule.

8.2 Motivation and Approach

A receiver without jitter compensation suffers significant BER degradation in colored timing jitters, especially when the jitter bandwidth is small, as discussed in Chapters 5 and 7. A new jitter compensation algorithm is proposed to improve the BER performance in colored Gaussian jitter when the jitter RMS value, ε_{rms}, and jitter bandwidth, f_L, of the system clock are known. In the proposed algorithm, the increase in correlation between successive jitter values as the jitter bandwidth decreases is exploited. By observing the decision variable for the present, n^{th} bit, the present jitter value may be tracked by making use of the pulse-template correlation function. Since successive jitter values are correlated, the tracked jitter value can be used together with the statistical properties of the clock to deduce significant statistical information on the decision variable of the next $n+1^{th}$ bit. This information can then be used together with the actual observed decision variable of the $n+1^{th}$ bit for bit detection using ML criterion.

The structure of the original receiver without jitter compensation is shown in Figure 8.1. This basic correlator receiver implements the binary Pulse Position Modulation bit detection as described in Chapter 4.

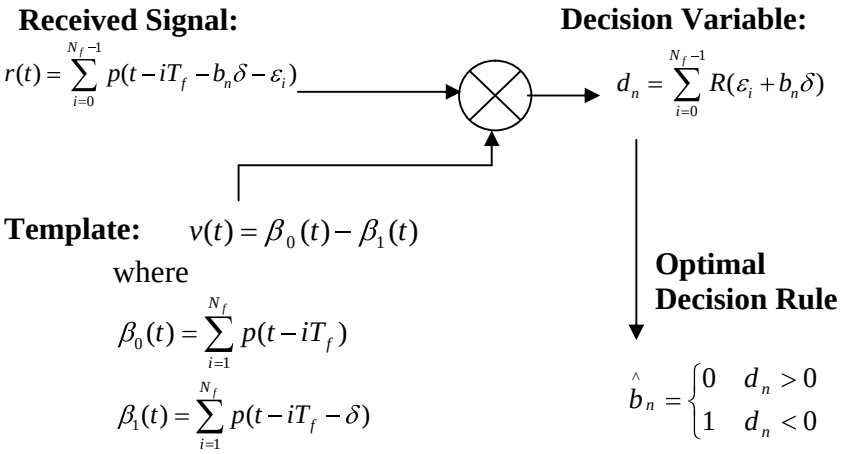

Figure 8.1: Original receiver without jitter compensation

In contrast, the structure of the new proposed receiver with jitter compensation is shown in Figure 8.2. It consists of a jitter tracker to track the n^{th} bit's jitter, ε_n, a jitter estimator to calculate the statistical properties of the estimate of the $n+1^{th}$ bit's jitter, $\hat{\varepsilon}_{n+1}$, and a new optimal ML decision rule.

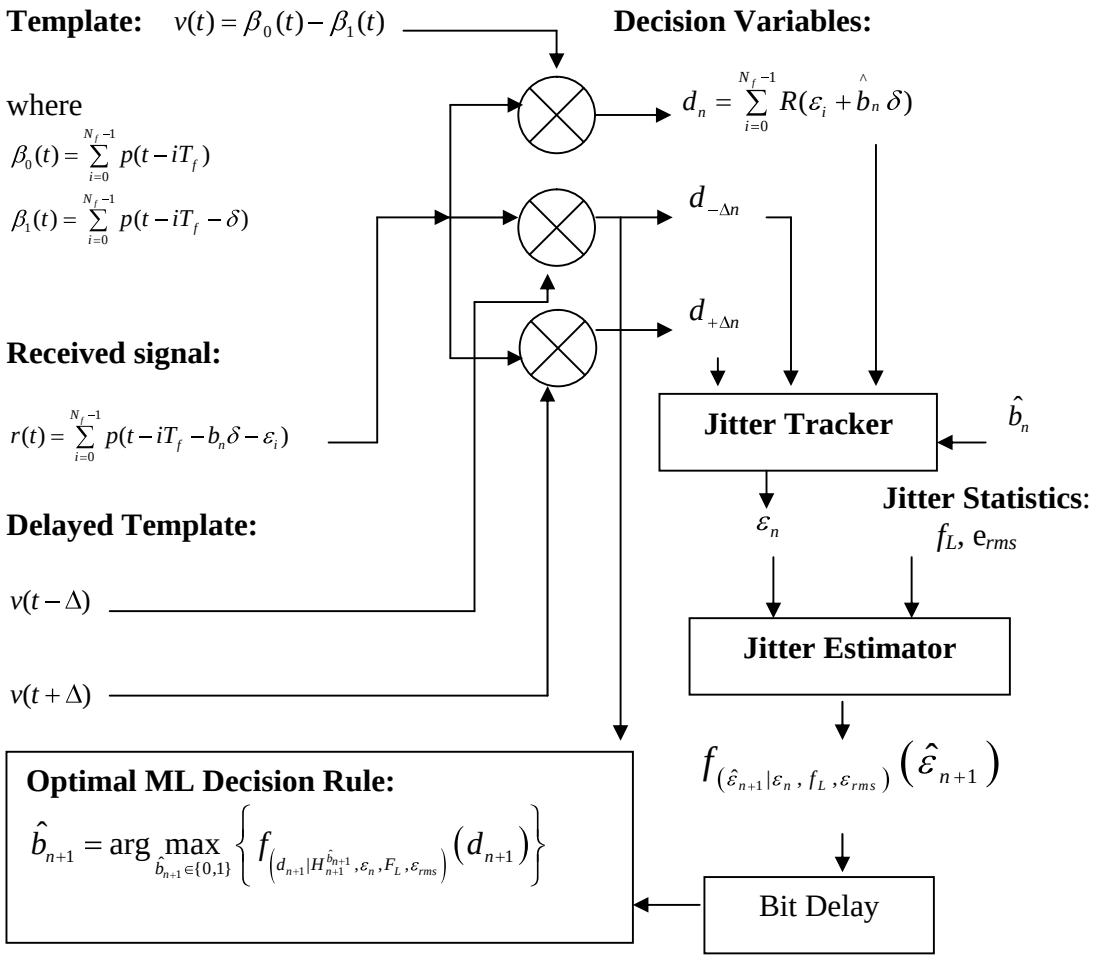

Figure 8.2: New receiver with jitter tracking and compensation

8.3 Jitter Tracker

In accordance with (5.2), the tracker aims to deduce information about the actual jitter value from the decision variable d_n. For the purpose of simplifying the algorithm, instead of deducing e_i for all i, we use the approximation that the jitter value, e_i, during the n^{th} bit's duration, is the same and denoted by e_n. As shown in Figure 8.3, such an approximation gets better as the jitter bandwidth f_L decreases. Based on the already decoded bit, $\hat{b}_n$, the tracked jitter value e_n for the n^{th} bit can be deduced. Due to the approximation, (5.2) becomes

$$d_n = N_f \cdot R(\varepsilon_n + \hat{b}_n \delta) . \tag{8.1}$$

How $\hat{b}_n$ can be obtained will be explained in greater detail in the next two sections concerning the jitter estimator and the ML decision rule. d_n is directly obtained from the correlator in the receiver. N_f and d are known variables and $R(t)$ is a known function in (5.1) and (4.3).

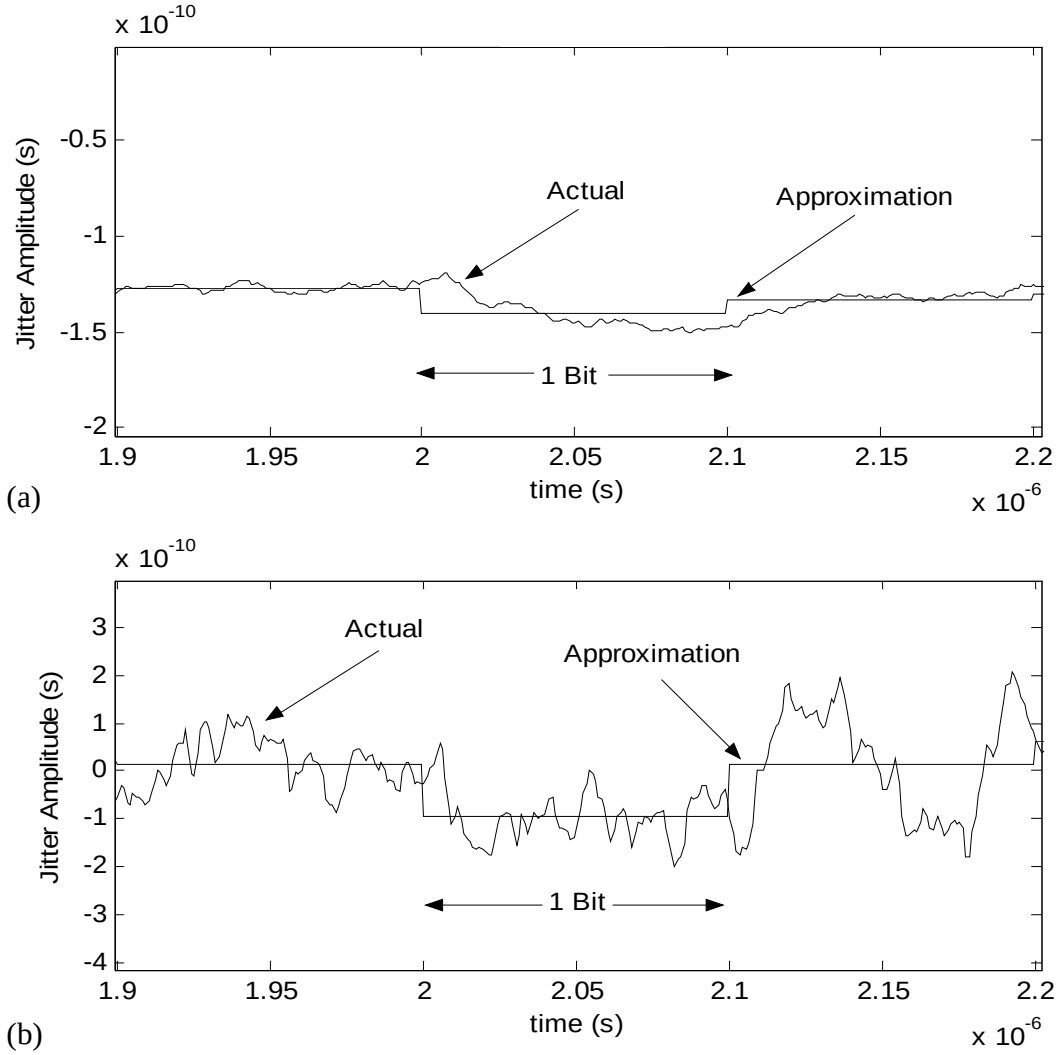

Figure 8.3: Approximation for jitter waveform (a) $f_L = 10^4$ Hz, (b) $f_L = 10^7$ Hz

The jitter is tracked by deducing e_n from the observed d_n as time progresses. From Figure 5.1, the pulse-template correlation function $R(t)$ is a many-to-one function. The mapping from d_n to e_n is thus not one-to-one, and each observed d_n results in a maximum of four possible values of e_n. This ambiguity can be resolved by performing three correlations between the received signal and the template instead of performing only one correlation. This is done by using two other templates with delays +? and –? respectively with respect to the original template. Thus (8.1) becomes

$$d_{-\Delta n} = N_f \cdot R(\varepsilon_n + \hat{b}_n \delta - \Delta) \tag{8.2}$$

and

$$d_{+\Delta n} = N_f \cdot R(\varepsilon_n + \hat{b}_n \delta + \Delta)\,. \tag{8.3}$$

The correlations of the received signal with the three relatively delayed templates are represented by (8.1), (8.2) and (8.3). Corresponding to each correlation, a solution set of four possible values of e_n may be deduced. The correct unambiguous solution for e_n corresponds to the solution which is common to all three sets, which is labeled as "$\tilde{\varepsilon}_n$" in Figure 8.4. In other words, based on the observed values of the decision variables d_n, $d_{-\Delta n}$ and $d_{+\Delta n}$, the jitter tracker solves for a unique e_n from (8.1), (8.2) and (8.3).

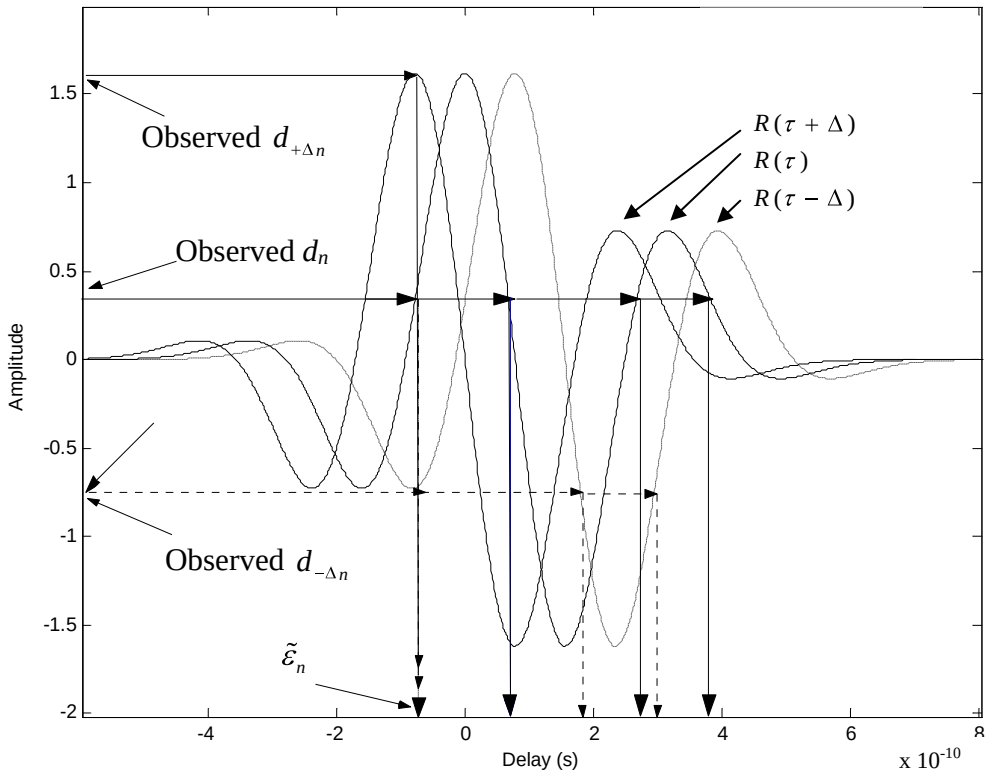

Figure 8.4: Resolving ambiguity for ε_n using three templates

8.4 Jitter Estimator

From the tracked jitter value e_n at the n^{th} bit, the statistical properties of the jitter estimate $\hat{\varepsilon}_{n+1}$ for the $n+1^{th}$ bit may be deduced. From the time domain representation of the jitter model in (6.19) and after some substitution and manipulation, it is observed that:

$$\varepsilon_0 = x_0 \cdot \frac{1}{1+\alpha} + x_{-1} \cdot \frac{1}{1+\alpha} + \varepsilon_{-1} \cdot \frac{\alpha - 1}{1+\alpha}$$

$$\varepsilon_1 = x_1 \cdot \frac{1}{1+\alpha} + x_0 \cdot \frac{2\alpha}{(1+\alpha)^2} + x_{-1} \cdot \frac{\alpha - 1}{(1+\alpha)^2} + \varepsilon_{-1} \cdot \frac{(\alpha - 1)^2}{(1+\alpha)^2}$$

$$\varepsilon_2 = x_2 \cdot \frac{1}{1+\alpha} + x_1 \cdot \frac{2\alpha}{(1+\alpha)^2} + x_0 \cdot \frac{2\alpha \cdot (\alpha-1)}{(1+\alpha)^3} + x_{-1} \cdot \frac{(\alpha-1)^2}{(1+\alpha)^3} + \varepsilon_{-1} \cdot \frac{(\alpha-1)^3}{(1+\alpha)^3}$$

$$\vdots$$

$$\varepsilon_i = x_i \cdot \frac{1}{1+\alpha} + \sum_{j=0}^{i-1} x_j \cdot \frac{2\alpha \cdot (\alpha-1)^{i-1-j}}{(1+\alpha)^{i+1-j}} + x_{-1} \cdot \frac{(\alpha-1)^i}{(1+\alpha)^{i+1}} + \varepsilon_{-1} \cdot \frac{(\alpha-1)^{i+1}}{(1+\alpha)^{i+1}}$$

$$\vdots$$

$$\varepsilon_{N_f-1} = x_{N_f-1} \cdot \frac{1}{1+\alpha} + \sum_{j=0}^{N_f-2} x_j \cdot \frac{2\alpha \cdot (\alpha-1)^{N_f-2-j}}{(1+\alpha)^{N_f-j}} + x_{-1} \cdot \frac{(\alpha-1)^{N_f-1}}{(1+\alpha)^{N_f}} + \varepsilon_{-1} \cdot \frac{(\alpha-1)^{N_f}}{(1+\alpha)^{N_f}}$$

,where *a* has been defined in (6.16). Averaging the value of the timing jitter at each pulse ε_i over all the N_f pulses in one bit and grouping together the coefficients of ε_{-1} and each x_i terms,

$$\varepsilon_{n+1} = \frac{1}{N_f} \sum_{i=0}^{N_f-1} \varepsilon_i = \frac{1}{N_f} \left\{ \begin{array}{l} \varepsilon_{-1} \cdot \left[\frac{\alpha-1}{1+\alpha} + \left(\frac{\alpha-1}{1+\alpha} \right)^2 + \left(\frac{\alpha-1}{1+\alpha} \right)^3 + \ldots + \left(\frac{\alpha-1}{1+\alpha} \right)^{N_f} \right] \\ + x_{-1} \cdot \left[\frac{1}{1+\alpha} + \frac{\alpha-1}{(1+\alpha)^2} + \frac{(\alpha-1)^2}{(1+\alpha)^3} + \ldots + \frac{(\alpha-1)^{N_f-1}}{(1+\alpha)^{N_f}} \right] \\ + x_0 \cdot \left[\frac{1}{1+\alpha} + \frac{2\alpha}{(1+\alpha)^2} + \frac{2\alpha(\alpha-1)}{(1+\alpha)^3} + \ldots + \frac{2\alpha(\alpha-1)^{N_f-2}}{(1+\alpha)^{N_f}} \right] \\ + x_1 \cdot \left[\frac{1}{1+\alpha} + \frac{2\alpha}{(1+\alpha)^2} + \frac{2\alpha(\alpha-1)}{(1+\alpha)^3} + \ldots + \frac{2\alpha(\alpha-1)^{N_f-3}}{(1+\alpha)^{N_f-1}} \right] \\ + x_2 \cdot \left[\frac{1}{1+\alpha} + \frac{2\alpha}{(1+\alpha)^2} + \frac{2\alpha(\alpha-1)}{(1+\alpha)^3} + \ldots + \frac{2\alpha(\alpha-1)^{N_f-4}}{(1+\alpha)^{N_f-2}} \right] \\ + \ldots\ldots \\ + x_{N_f-2} \cdot \left[\frac{1}{1+\alpha} + \frac{2\alpha}{(1+\alpha)^2} \right] \\ + x_{N_f-1} \cdot \left[\frac{1}{1+\alpha} \right] \end{array} \right\} \quad (8.4)$$

The jitter estimate $\hat{\varepsilon}_{n+1}$ of the $n+1^{th}$ bit may thus be written as

$$\begin{aligned}\hat{\varepsilon}_{n+1} &= \frac{1}{N_f}\sum_{i=0}^{N_f-1}\varepsilon_i \\ &= \frac{1}{N_f}\left[\varepsilon_n\sum_{j=1}^{N_f}\left(\frac{\alpha-1}{1+\alpha}\right)^j + x_{-1}\sum_{j=1}^{N_f}\frac{(\alpha-1)^{j-1}}{(1+\alpha)^j} + \sum_{i=0}^{N_f-2}x_i\left(\sum_{j=1}^{N_f-i-1}\frac{2\alpha(\alpha-1)^{j-1}}{(1+\alpha)^{j+1}} + \frac{1}{1+\alpha}\right) + x_{N_f-1}\frac{1}{1+\alpha}\right]\end{aligned}$$

. (8.5)

Note that ε_{-1} is the same as ε_n, the timing jitter associated with the n^{th} bit. This is due to the approximation mentioned in the previous section.

Defining

$$\begin{aligned}\sigma_{\varepsilon_n} &= \sum_{j=1}^{N_f}\left(\frac{\alpha-1}{1+\alpha}\right)^j \\ \sigma_{x_{-1}} &= \sum_{j=1}^{N_f}\frac{(\alpha-1)^{j-1}}{(1+\alpha)^j} \\ \sigma_{x_i} &= \sum_{j=1}^{N_f-i-1}\frac{2\alpha(\alpha-1)^{j-1}}{(1+\alpha)^{j+1}} + \frac{1}{1+\alpha},\ i=1,2,\cdots,N_f-1 \\ \sigma_{x_{N_f-1}} &= \frac{1}{1+\alpha},\end{aligned}$$

(8.5) becomes

$$\hat{\varepsilon}_{n+1} = \frac{1}{N_f}\left(\sigma_{\varepsilon_n}\varepsilon_n + \sigma_{x_{-1}}x_{-1} + \sigma_{x_0}x_0 + \sigma_{x_1}x_1 + \ldots + \sigma_{x_{N_f-1}}x_{N_f-1}\right). \quad (8.6)$$

Since the random variables x_i (i = -1, 0, 1, …, $N_f - 1$) are white Gaussian, $\hat{\varepsilon}_{n+1}$ is a weighted sum of white Gaussian samples. The PDF of $\hat{\varepsilon}_{n+1}$ is thus Gaussian and can be written as:

$$f_{(\hat{\varepsilon}_{n+1}|\varepsilon_n, f_L, \varepsilon_{rms})}\left(\hat{\varepsilon}_{n+1}\right) = N\left(\frac{1}{N_f}\sigma_{\varepsilon_n}\varepsilon_n,\ \frac{\sigma_x^2}{N_f^2}\left(\sigma_{x_{-1}}^2 + \sigma_{x_0}^2 + \sigma_{x_1}^2 + \ldots + \sigma_{x_{N_f-1}}^2\right)\right) \quad (8.7)$$

where σ_x^2, the variance of the white Gaussian samples x, is given in (6.24). The s terms in (8.7) is a function of a. Furthermore from Chapter 6, a depends on f_L and σ_x^2 depends

on f_L and ε_{rms}. Thus the PDF of $\hat{\varepsilon}_{n+1}$ is conditional upon the tracked jitter ε_n, the jitter bandwidth f_L, and the jitter RMS value ε_{rms}. Figure 8.5 shows the theoretical PDF of $\hat{\varepsilon}_{n+1}$ plotted together with the actual histogram generated from 10^6 samples of $\hat{\varepsilon}_{n+1}$ for the same parameters ε_n, f_L, and ε_{rms}, thereby verifying (8.7).

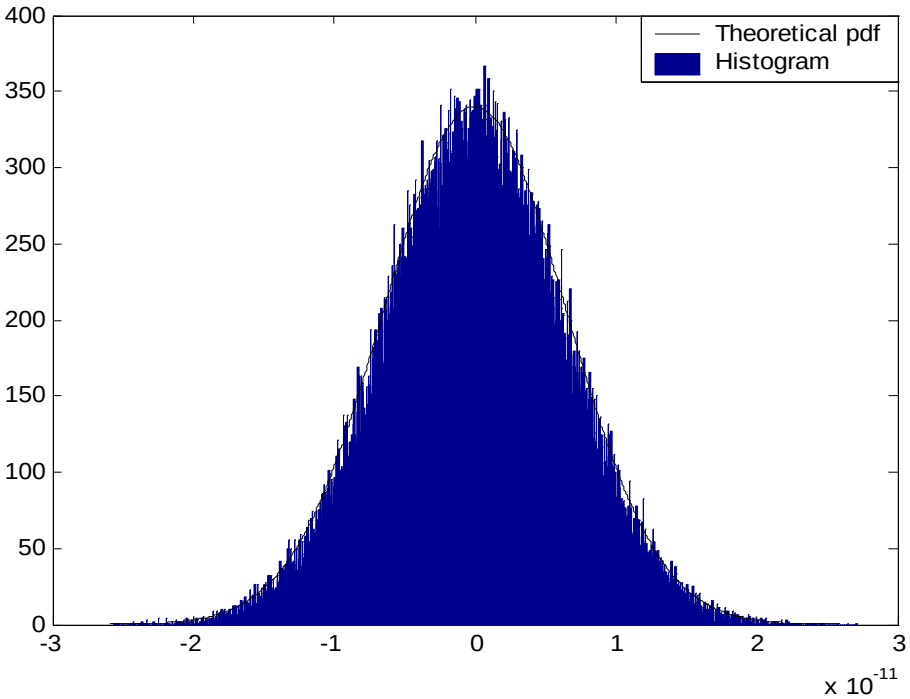

Figure 8.5: Probability Distribution Function of $\hat{\varepsilon}_{n+1}$

Hence the jitter estimator deduces the statistics of the jitter estimate, $\hat{\varepsilon}_{n+1}$, of the $n+1^{th}$ bit from the tracked jitter value, ε_n, of the n^{th} bit.

8.5 Optimum ML Decision Rule

The PDF of the decision variable d_{n+1}, conditioned upon either of the two hypotheses for the $n+1^{th}$ bit is required for the formulation of a ML decision rule to

detect the $n+1^{th}$ bit. Corresponding to bit '0' and bit '1', the hypotheses can be denoted by $H_{n+1}^{\hat{b}_{n+1}}$ where $\hat{b}_{n+1}=0$ or $\hat{b}_{n+1}=1$.

Thus from (8.1),

$$d_{n+1} = N_f \cdot R(\hat{\varepsilon}_{n+1} + \hat{b}_{n+1} \cdot \delta) . \tag{8.8}$$

Given the PDF of $\hat{\varepsilon}_{n+1}$ from the previous section, the PDF of the decision statistics d_{n+1} may conceivably be obtained for the ML decoding of the $n+1^{th}$ bit.

There is a crucial difference between (8.1) and (8.8). (8.8) is used to obtain the ML estimate for $\hat{b}_{n+1}$, ie. the $n+1^{th}$ bit, after having obtained the timing jitter estimate $\hat{\varepsilon}_{n+1}$ associated with the $n+1^{th}$ bit (the jitter estimator estimates $\hat{\varepsilon}_{n+1}$ from the tracked jitter value ε_n associated with the n^{th} bit). (8.1) is used to track the ε_n associated with the n^{th} decoded bit after the n^{th} decoded bit has been earlier estimated with (8.8) using the tracked timing jitter ε_{n-1} associated with the $n-1^{th}$ bit.

Obviously, the d_{n+1} in (8.8) is a function of $\hat{\varepsilon}_{n+1}$ which is a Gaussian distributed random variable. It thus has a non-Gaussian PDF. Furthermore corresponding to the two possible hypotheses for $\hat{b}_{n+1}$, d_{n+1} has two possible PDFs. Based on the two possible PDFs, the ML approach selects the more probable hypothesis based on the actual d_{n+1} obtained from performing correlation between the received signal and the template.

Using transformation of PDF, the PDF of d_{n+1} is given by

$$f_{\left(d_{n+1}|H_{n+1}^{\hat{b}_{n+1}},\varepsilon_n,f_L,\varepsilon_{rms}\right)}\left(d_{n+1}\right) = \sum f_{\left(\hat{\varepsilon}_{n+1}|\varepsilon_n,f_L,\varepsilon_{rms}\right)}\left(\hat{\varepsilon}_{n+1}\right) \cdot \left| \frac{\partial R^{-1}\left(d_{n+1}/N_f\right)}{\partial d_{n+1}} \right|, \tag{8.9}$$

where the summation is taken over all the regions defined by the roots of $R^{-1}(d_{n+1}/N_f)$, and $R(t)$ is the pulse-template correlation function as defined in (5.1) and (4.3). In other words $R(t)$ is the mapping function between d_{n+1} and $\hat{\varepsilon}_{n+1}$,

$$d_{n+1} = R(\hat{\varepsilon}_{n+1}). \tag{8.10}$$

The PDF of d_{n+1} cannot be obtained in closed form as it involves the inversion of the pulse-template correlation function, $R(t)$, which is mathematically intractable. However, this PDF can be evaluated numerically in MATLAB. The decision rule for the $n+1^{th}$ bit according to the ML criterion is:

$$\hat{b}_{n+1} = \arg \max_{\hat{b}_{n+1} \in \{0,1\}} \left\{ f_{\left(d_{n+1} | H_{n+1}^{\hat{b}_{n+1}}, \varepsilon_n, f_L, \varepsilon_{rms}\right)} \left(d_{n+1}\right) \right\}, \tag{8.11}$$

The probability density functions, $f(d_{n+1})$ corresponding to both hypotheses in the decision rule changes as the jitter is tracked, and the optimum decision rule in (8.11) may be implemented as the dynamic updating of the decision threshold, D_T, in the receiver to reduce online computational complexities. The decision threshold, D_T, is a threshold value to make a decision for bit '0' or bit '1'. It partitions the local decision variable region into two or more distinct regions about the threshold. If the decision variable takes on values greater than D_T, a decision is made for bit '0' and vice versa.

Figure 8.6a shows the probability density functions of the two hypotheses *H0* and *H1* when the tracked jitter, e_n, is zero. In this particular case the decision threshold, D_T, is zero and the decision region is identical to that in (4.6). This is the case always assumed always by the original receiver since it does not track the jitter. As time progresses, the tracked jitter, e_n, changes its value randomly. Since the two probability density functions

of d_{n+1} are conditional upon ε_n, f_L, and ε_{rms}, both the decision threshold and the decision regions will change accordingly.

In Figure 8.6b, the decision threshold, D_T, shifts left and the decision regions change accordingly. In Figure 8.6c, there are two decision thresholds, D_{T1} and D_{T2} and three decision regions. In this case, the receiver makes a decision for bit '1' if the actual observed d_{n+1} falls in the region between D_{T1} and D_{T2}.

A table of a set of D_T, corresponding to the value of the tracked jitter, e_n, and given the jitter bandwidth and jitter RMS value of the system clock, may be pre-calculated and stored at the receiver thereby saving the computational complexity associated in the calculation of the probability density functions of d_{n+1} online.

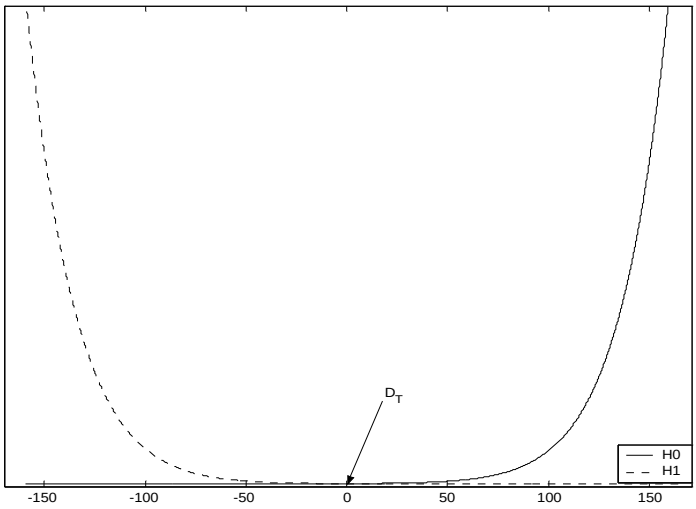

Fig. 8.6(a): Probability density functions of d_{n+1} when e_n =0 ps and the associated decision thresholds and regions.

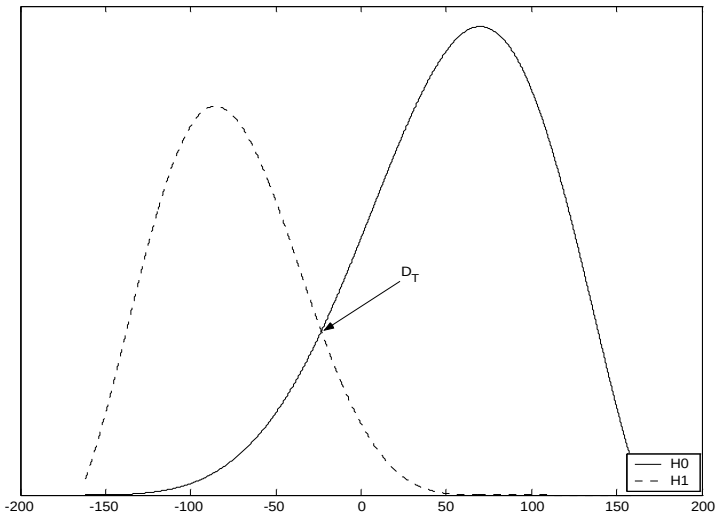

Fig. 8.6(b): Probability density functions of d_{n+1} when e_n =56 ps and the associated decision thresholds and regions.

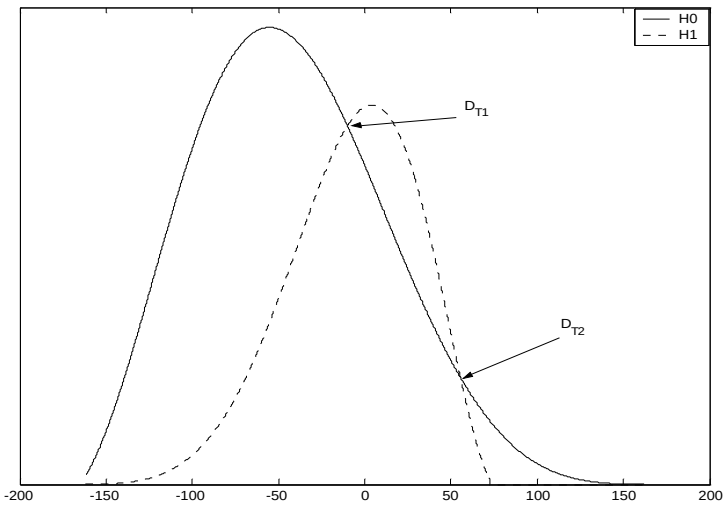

Fig. 8.6(c): Probability density functions of d_{n+1} when e_n =95 ps and the associated decision thresholds and regions.

8.6 Performance Evaluation and Discussion

Using the same set of simulation parameters in Chapter 7, the performance of the proposed jitter compensation algorithm is evaluated. Figure 8.7 shows the simulated BER curves in colored timing jitters with bandwidth ranging from 10^4 Hz to 10^6 Hz. The results without compensation are also plotted for comparison.

The simulation results in Figure 8.7 shows that the proposed algorithm results in a significant improvement in BER performance. Notably at the same jitter RMS value, the improvement in BER performance is more significant as the jitter bandwidth decrease. At a jitter RMS value of 60 ps, a significant improvement in BER performance of approximately one order of magnitude and half an order of magnitude is achieved for jitter with bandwidth of 10^4 Hz and 10^5 Hz. As the jitter bandwidth increases to 10^6 Hz, the improvement in BER performance is less significant. This is not surprising since the proposed algorithm exploits the increased correlation in the timing jitter to enhance BER performance and the jitter correlation is less significant at higher bandwidth.

As can be seen from Figure 8.7, the improvement in BER performance is also more significant as the jitter RMS value increases for the same jitter bandwidth. For the same jitter bandwidth of 10^4 Hz, an improvement in BER performance of approximately one order of magnitude is achieved for jitter RMS value of 40 ps and above. However for jitter RMS value lesser than 40 ps, the improvement in BER performance rapidly decreases. This is not surprising since the proposed algorithm's capability for tracking the jitter to improve BER performance is better exploited at the higher jitter RMS values.

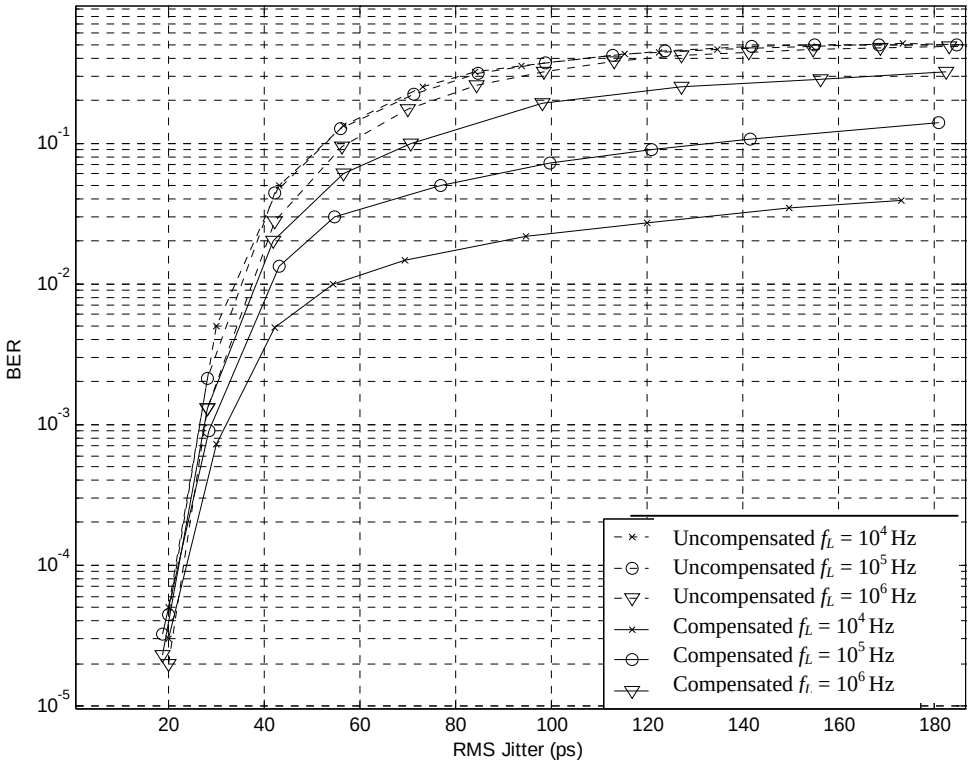

Figure 8.7: BER performance after jitter compensation

8.7 Computation Complexity of the proposed Jitter Compensation Algorithm

Comparing Figure 8.1 and Figure 8.2, the added complexity of the proposed algorithm results mainly from the additional Jitter Tracker and Jitter Estimator blocks.

The Jitter Estimation block and the new ML decision rule in (8.11) do not incur additional computational complexity if the decision threshold, D_T, is pre-tabulated (after examining the PDF of the decision variables in accordance to (8.9)) and loaded into the

receiver's memory in the form of Look-Up-Tables (LUTs) implementation. The only parameter to be calculated online is thus e_n. This occurs at the Jitter Tracker block.

At the Jitter Tracker block, the increase in computational complexity arises from the need to calculate e_n, the jitter value at the *nth* bit, in accordance to (8.1), (8.2) and (8.3) and Figure 8.4. This results in the computationally intensive reversal of the three equations (8.1) to (8.3), followed by finding a unique solution among the three sets of (at most) 4 solutions. In actual hardware implementation, Look-Up-Tables (LUTs) describing the three equations may be pre-calculated once and loaded up into the receiver's memory. This removes the need for the computationally intensive calculation. A simple analysis will show that the maximum number of comparisons required to find the unique solution common to the three sets (up to four solutions each) is twenty-three.

Hence the added complexity of the jitter compensated receiver is that memory is needed to store the above mentioned LUTs and that an additional twenty three comparisons per bit is needed in the worst case scenario.

CHAPTER 9

CONCLUSION AND FUTURE WORKS

9.1 Conclusion

The problem that is being addressed in this thesis is the effect of clock timing jitter on the BER performance of a UWB system that uses binary Pulse Position Modulation. Practical system clocks exhibit colored timing jitter. In this thesis, the clock is characterized by its jitter bandwidth and jitter RMS value.

The effect of colored timing jitter on the BER performance of a single-user binary PPM UWB system has been quantified, showing that BER performance is significantly worse in colored timing jitter than in white jitter and that the extent of BER degradation increases as the jitter bandwidth decreases. A jitter RMS value of 105ps for white jitter results in a BER of 10^{-3}, while for colored jitter with 3 dB bandwidth of 10^{5} Hz, a significantly smaller jitter RMS value of 25ps results in the same BER. The upper and lower BER bounds over all jitter bandwidths have also been derived and verified by simulation.

A new jitter compensation algorithm has been proposed in response to the above results to improve BER performance in colored Gaussian timing jitter. Simulation results using typical parameter settings found in literature show that the proposed algorithm is effective in improving the BER performance in colored timing jitter. The improvement in BER performance is more significant as the jitter bandwidth decreases and as the jitter

RMS value increases. The improvement is as large as one order of magnitude for the lower jitter bandwidths beyond a jitter RMS value of 40 ps.

9.2 Future Works

Future works could include the effects of clock timing jitters to the problem of UWB channel estimation. An important work has been presented in literature describing a maximum-likelihood (ML) approach to estimate the channel parameters (the delays and attenuation associated with each channel paths) [22]. Several recent works have also focused on low-complexity algorithms for rapid timing acquisition [23][24][25]. However none has included the effects of clock timing jitter in the channel estimation problem formulation. Since the presence of clock timing jitter affects the channel delays estimations, it will be of interest and importance to investigate the joint channel delay-clock timing jitter problem.

BIBLIOGRAPHY

[1] R. A. Scholtz, "Multiple access with time-hopping impulse modulation," in *Proc. IEEE MILCOM 1993*, Oct. 1993, vol. 2, pp.447-450.

[2] M. Z. Win and R. A. Scholtz, "Ultra-wide bandwidth time-hopping spread-spectrum impulse radio for wireless multiple-access communications," *IEEE Trans. Commun.*, vol. 48, pp.679-691, Apr. 2000.

[3] F. Ramfrez-Mireles, "Signal design for ultra-wide-band communications in dense multipath," *IEEE Trans. Veh. Technol.*, vol. 51, pp. 1517-1521, Nov. 2002.

[4] M. Z. Win and R. A. Scholtz, "Characterization of ultra-wide bandwidth wireless indoor channels: a communication-theoretic view," *IEEE J. Select. Areas Commun.*, vol. 20, pp. 1613-1627, Dec. 2002.

[5] L. Huang and C. C. Ko, "Performance of maximum-likelihood channel estimator for UWB communications," *IEEE Commun. Lett.*, vol. 8, pp. 356-358, Jun. 2004.

[6] L. Yang and G. B. Giannakis, "Optimal pilot waveform assisted modulation for ultrawideband communications," *IEEE Trans. Wireless Commun*., vol. 3, pp. 1236-1249, Jul. 2004.

[7] L. Yang and G. B. Giannakis, "Analog space-time coding for multiantenna ultra-wideband transmission," *IEEE Trans. Commun.*, vol. 52, pp. 507-517, Mar. 2004.

[8] E. Fishler and H. V. Poor, "Low-complexity multiuser detectors for time-hopping impulse-radio systems," *IEEE Tran. Signal Processing*, vol. 52, pp. 2561-2571, Sept. 2004.

[9] M. Hamalainen, V. Hovinen, R. Tesi, J. H. J. Iinatti and M. Latva-aho, "On the UWB system coexistence with GSM900, UMTS/WCDMA, and GPS," *IEEE J. Select. Areas Commun.*, vol. 20, pp.1712 –1721, Dec. 2002.

[10] L. Zhao and A. M. Haimovich, "Performance of ultra-wideband communications in the presence of interference," *IEEE J. Select. Areas Commun.*, vol. 20, pp. 1684-1691, Dec. 2002.

[11] W. M. Lovelace and J. K. Townsend, "The effects of timing jitter and tracking on the performance of impulse radio," *IEEE J. Select. Areas Commun.*, vol. 20, pp. 1646-1651, Dec. 2002.

[12] J. A. Mcneill, "A simple method for relating time and frequency-domain measures of oscillator performance," in *Proc. Southwest Symposium on Mixed-Signal Design*, Feb. 2001, pp.7 –12.

[13] Federal Communications Commission's (FCC) Report and Order (R&O), issued April 2002

[14] Paul Withington, "Impulse Radio Overview", Time Domain Corp, 2002

[15] "New" Ultra-wideband technology White Paper, Prepared by Discrete Time Communications, Oct. 2002

[16] M. Z. Win and R. A. Scholtz, "On the robustness of ultra-wide bandwidth signals in dense multipath environment, *IEEE Communs Letters*, vol. 2, No. 2, pp.51-53, Feb 1998

[17] Dr. R. J. Fontana and S. J. Gundersun, "UWB Precision Asset Location System," in *Proc. IEEE UWBST 2002*, May 2002, pp. 147-150

[18] Multispectral.com, UWBFAQ, Advantages of UWB, www.multispectral.com/UWBFAQ.html

[19] D. Kelly, S. Reinhardt, R. Stanley and M. Einhorn, "PulsON second generation timing chip: enabling UWB through precise timing," in *Proc. IEEE UWBST 2002*, May 2002, pp. 117-122.

[20] F. Ramfrez-Mireles and R. A. Scholtz, "System performance analysis of impulse radio modulation," in *Proc. IEEE RAWCON 1998*, Aug. 1998, pp.123-127.

[21] Simon Haykins, Digital Communications, John Wiley & Sons, Inc, pp.340 (1998)

[22] V.Lottici, A.D'Andrea and U. Mengali, "Channel estimation for ultra-wideband communications." *IEEE J. Selected Areas Comm.*, vol. 20, no. 12, pp.1638-1645, Dec.2002

[23] R. Blazquez, P. Newaskar and A. Chandrakasan, "Coarse Acquisition for Ultra Wideband Digital Receivers," *IEEE ICASSP'2003*, Apr. 2003.

[24] R. Fleming, C. Kushner, G. Roberts and U. Nandiwada, "Rapid acquisition for ultra- wideband localizers," *IEEE Conf. on UWB Systems & Tech.*, Baltimore, MD, pp. 245-250, May 2002.

[25] L. Yang, Z. Tian, and G. B. Giannakis, "Non-Data-Aided Timing Acquisition of UWB Signals Using Cyclostationarity," *IEEE ICASSP'03*, Apr. 2003.